Journal of Nanobiotechnology

RESEARCH

Open Access

Oral enzyme-responsive nanoprobes for targeted theranostics of inflammatory bowel disease

Lin Cao[1†], Dengyi Duan[1†], Jing Peng[1†], Ruinan Li[4], Qi Cao[5], Xinwen Li[1], Yunfei Guo[1], Jianmin Li[2,3], Kangkang Liu[2], Yiming Li[1], Wenyi Zhang[1], Shuang Liu[1], Xuening Zhang[1] and Yang Zhao[1,2*]

Abstract

Background Inflammatory bowel disease (IBD) is a progressive and debilitating inflammatory disease of the gastrointestinal tract (GIT). Despite recent advances, precise treatment and noninvasive monitoring remain challenging.

Methods Herein, we developed orally-administered, colitis-targeting and hyaluronic acid (HA)-modified, core-shell curcumin (Cur)- and cerium oxide (CeO_2)-loaded nanoprobes (Cur@PC-HA/CeO_2 NPs) for computed tomography (CT) imaging-guided treatment and monitoring of IBD in living mice.

Results Following oral administration, high-molecular-weight HA maintains integrity with little absorption in the upper GIT, and then actively accumulates at local colitis sites owing to its colitis-targeting ability, leading to specific CT enhancement lasting for 24 h. The retained NPs are further degraded by hyaluronidase in the colon to release Cur and CeO_2, thereby exerting anti-inflammatory and antioxidant effects. Combined with the ability of NPs to regulate intestinal flora, the oral NPs result in substantial relief in symptoms. Following multiple treatments, the gradually decreasing range of the colon with high CT attenuation correlates with the change in the clinical biomarkers, indicating the feasibility of treatment response and remission.

Conclusion This study provides a proof-of-concept for the design of a novel theranostic integration strategy for concomitant IBD treatment and the real-time monitoring of treatment responses.

Keywords Inflammatory bowel disease, Colitis-targeting, Cerium oxide nanozyme, CT imaging, Microflora regulation

†Lin Cao, Dengyi Duan and Jing Peng contributed equally to this work.

*Correspondence:
Yang Zhao
yang.zhao@tmu.edu.cn
[1]Department of Radiology, The Second Hospital of Tianjin Medical University, Tianjin 300211, China
[2]Tianjin Institute of Urology, The Second Hospital of Tianjin Medical University, Tianjin 300211, China
[3]Tianjin Key Laboratory of Precision Medicine for Sex Hormones and Diseases (in Preparation), The Second Hospital of Tianjin Medical University, Tianjin 300211, China
[4] Image Center, Cangzhou Hospital of Integrated and Western Medicine, Cangzhou 061001, China
[5]Department of Reproductive Medicine, First Teaching Hospital of Tianjin University of Traditional Chinese Medicine, Tianjin 300380, China

Introduction

Inflammatory bowel disease (IBD), which mainly comprises ulcerative colitis (UC) and Crohn's disease (CD), is a group of chronic, progressive, and debilitating inflammatory disorders of unknown origin in the gastrointestinal tract (GIT). The prevalence of IBD has substantially increased between 1990 and 2017, affecting approximately 6.8 million patients worldwide [1]. Various treatment options have been introduced for IBD, including aminosalicylates, corticosteroids, immunomodulators, and biologics [2, 3]. However, a large proportion of patients fail to achieve clinical remission with these treatments, or lose response over time, leading to adverse complications such as opportunistic infections, malignancies, autoimmune disorders, hepatotoxicity or nephrotoxicity [4, 5]. Moreover, IBD is highly heterogeneous, with recurrent, relapsing, and remitting course. Thus, patients often require life-long treatment for symptom management, which greatly affects their quality of life. Therefore, timely and personalized treatment adjustments are necessary, which are based on a comprehensive evaluation of multiple factors, including disease severity, treatment response, and overall health condition. Unfortunately, predicting the disease course and treatment response and thereby establishing optimal treatment choices is challenging. Hence, a novel theranostic strategy is highly desirable for IBD that can provide effective treatment and real-time assessment of the disease state and monitor therapy response for precise management and timely therapy adjustment of IBD.

In recent years, the application of non-invasive radiological imaging in the clinical examination of IBD has received increasing attention. Several studies have demonstrated the potential of nanoparticles that based on fluorescence imaging in IBD theranostics, however, these nanoparticles are not applicable to living animals owing to their inability for sufficient deep penetration of intra-abdominal tissues [6, 7]. Computed tomography (CT) is a widely used diagnostic and monitoring tool in clinical practice, particularly for abdominal disease [8–11]. Compared with fluorescence imaging, CT possesses the advantages of high resolution, short examination time, unlimited tissue penetration, and three-dimensional (3D) visualization of the target tissue [11, 12]. However, to the best of our knowledge, no reports exist on CT-visualized theranostics for IBD owing to the lack of colon specificity for small molecule iodine-based CT contrast agents. Among the alternative CT contrast agents being investigated, cerium oxide (CeO_2) nanoparticles, with a K-edge at 40.4 keV, has been demonstrated as a CT contrast agent for imaging gastrointestinal inflammation [13, 14]. In addition, the presence of both Ce^{3+} and Ce^{4+} sites on the surface of CeO_2 nanoparticles endows them with nanozymes activity, allowing them to catalyze the removal of various reactive oxygen species (ROS) [15, 16]. Moreover, its nanozymes activity can effectively reduce the free radicals generated at the inflammatory site and promote inflammation recovery compared with traditional contrast agents. Therefore, CeO_2 is considered a promising CT contrast agent for imaging gastrointestinal inflammation.

Recently, colon-targeted oral delivery nanoparticles (NPs) has been considered to be one of the most promising clinical translational methods, owing to their potential for greater dosage flexibility, convenience of self-administration, and patient compliance [17]. Curcumin (Cur) is a natural bioactive polyphenol derived from the turmeric rhizome. Due to its attractive anti-inflammatory and antioxidant pharmacological activities, Cur can relieve IBD by regulating related inflammatory signaling pathways and repairing the intestinal epithelial barrier [18, 19]. However, it has been limited as a clinical therapeutic drug due to low potency, poor solubility, poor absorption, low biodistribution [20–22]. To improve the bioavailability of Cur, poly (lactide-co-glycolic acid) (PLGA) was used as the cargo carrier to encapsulate it within NPs. However, the PLGA particle system alone is subject to partial degradation in the acidic environment of the stomach and, thus, the coating or functionalization of the drug-PLGA core with polysaccharides to protect the drug degradation in the acidic environment is essential to enhance the therapeutic response at the colitis site.

Hyaluronic acid (HA), a natural polysaccharide commonly found in the synovial fluid and extracellular matrix, can specifically bind to CD44 receptors that are highly expressed on the surfaces of colon inflammatory or tumor cells [23]. After oral administration, HA with high molecular weight can be selectively absorbed in the large intestine, whereas the small molecules of HA scarcely reach the lower GIT owing to their non-specific absorption by natural human metabolism, such as the portal vein and lymph vessels in the gastrointestinal sites [24]. Furthermore, various studies have demonstrated that HA-based NPs can improve the dysregulated intestinal barrier, microbiome, and immune responses in colitis [25–27].Therefore, HA may be an ideal carrier for targeting colitis.

In this study, we report a novel and effective colitis-targeted oral delivery system, HA-modified, core–shell curcumin (Cur)- and CeO_2-loaded NPs (Cur@PC-HA/CeO_2 NPs), for the CT imaging-guided theranostics of IBD. Cur, a harmless natural polyphenol compound widely used in the treatment of IBD [20, 21], was chosen as the model drug for encapsulation within NPs by poly(lactide-co-glycolic acid) (PLGA). In addition, HA polysaccharide as a template loaded with cerium to form HA/CeO_2 nanozyme. Subsequently, the drug-PLGA core was coated with chitosan polysaccharides to form Cur@

PC NPs with amines (+) on the surface, allowing the drug-PLGA cores to combine with the nanozyme HA/CeO_2 to synthesize core–shell drug-loaded nanoprobes (Cur@PC-HA/CeO_2) via amide bond binding between HA and chitosan in the outer layer. Thus, this novel theranostic integration strategy might allow for concomitant real-time diagnosis and therapy, holding great promise as a potential approach for effective and personalized management of IBD.

Results and discussion

Synthesis and characterization

The preparation of Cur@PC-HA/CeO_2 is briefly described as follows: First, Cur@PLGA cores were prepared using an emulsion/solvent evaporation method to convert Cur into PLGA, one of the most widely investigated biocompatible and biodegradable synthetic polymers with various biomedical applications in humans [28–30]. Chitosan polysaccharides were subsequently coated onto the Cur@PLGA cores to form Cur@PC NPs with amines (+) on the surface (Fig. 1A, Additional file 1: Fig. S1). Dynamic light scattering (DLS) measurements were performed to verify successful surface coating, which revealed that the hydrodynamic diameter of the prepared Cur@PC NPs increased by approximately 40 nm compared with that of the uncoated Cur@PLGA NPs cores (Additional file 1: Fig. S2-S5), while the surface zeta potential turned from negative (−16.83±0.15 mV) to positive (+12.43±1.44 mV; Fig. 2A). Finally, ceria nanozymes (HA/CeO_2) synthesized with HA polysaccharides as a template were coupled with Cur@PC NPs through amide bond binding between the HA and chitosan in the outer layer (Fig. 1A). The zeta potential of the resultant NPs (Cur@PC-HA/CeO_2) became negative (−46.97±2.65 mV; Fig. 2A), with an increased hydrodynamic diameter of approximately 270 nm (Fig. 2B). Fourier transform infrared spectroscopy of Cur@PC-HA/CeO_2 NPs was performed to confirm the successful conjugation of Cur@PC and HA/CeO_2 NPs. New peaks at 1759 and 1420 cm^{-1} could be assigned to –C=O and –C–N groups, respectively, on HA functionalized NPs

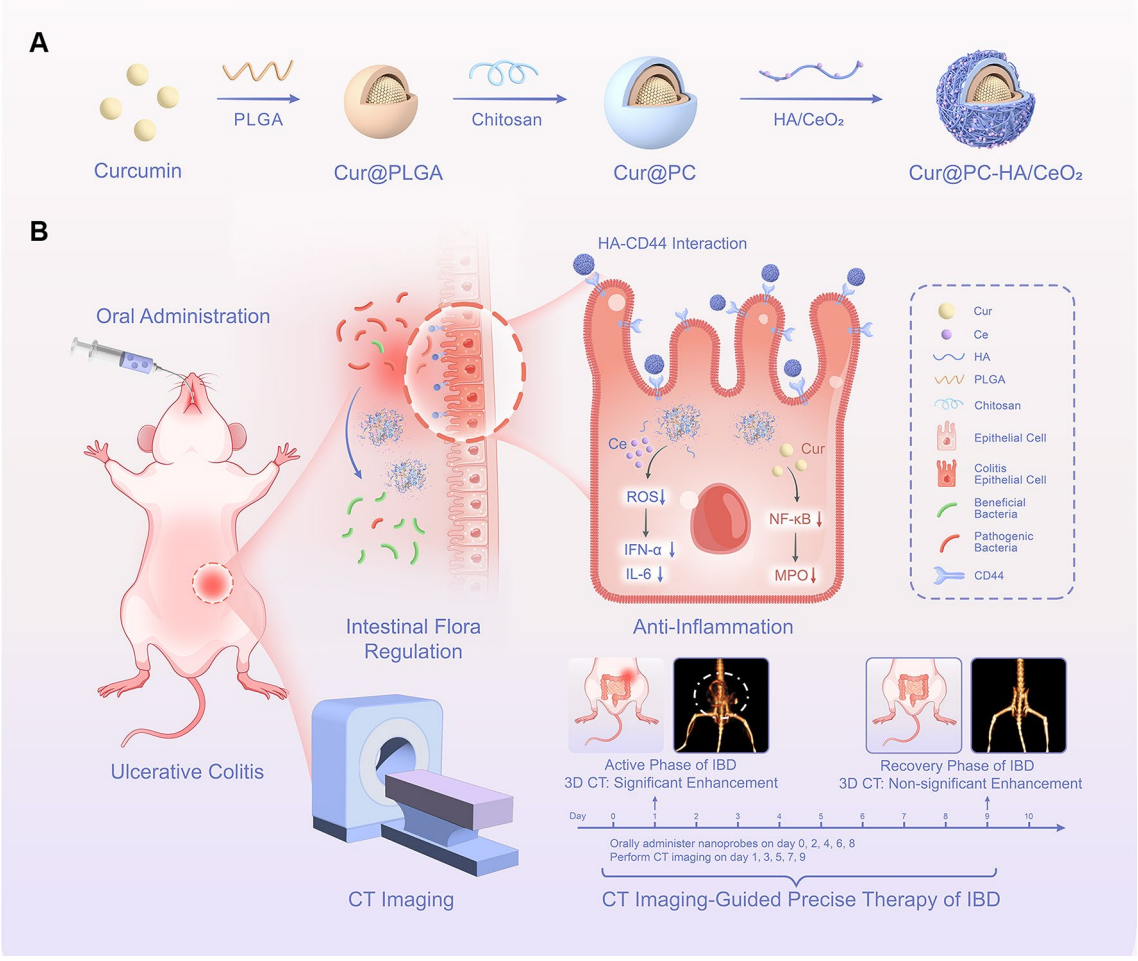

Fig. 1 (**A**) Preparation process of Cur@PC-HA/CeO_2 nanoprobes. (**B**) Schematic illustration of the application of Cur@PC-HA/CeO_2 nanoprobes for inflammatory bowel disease treatment

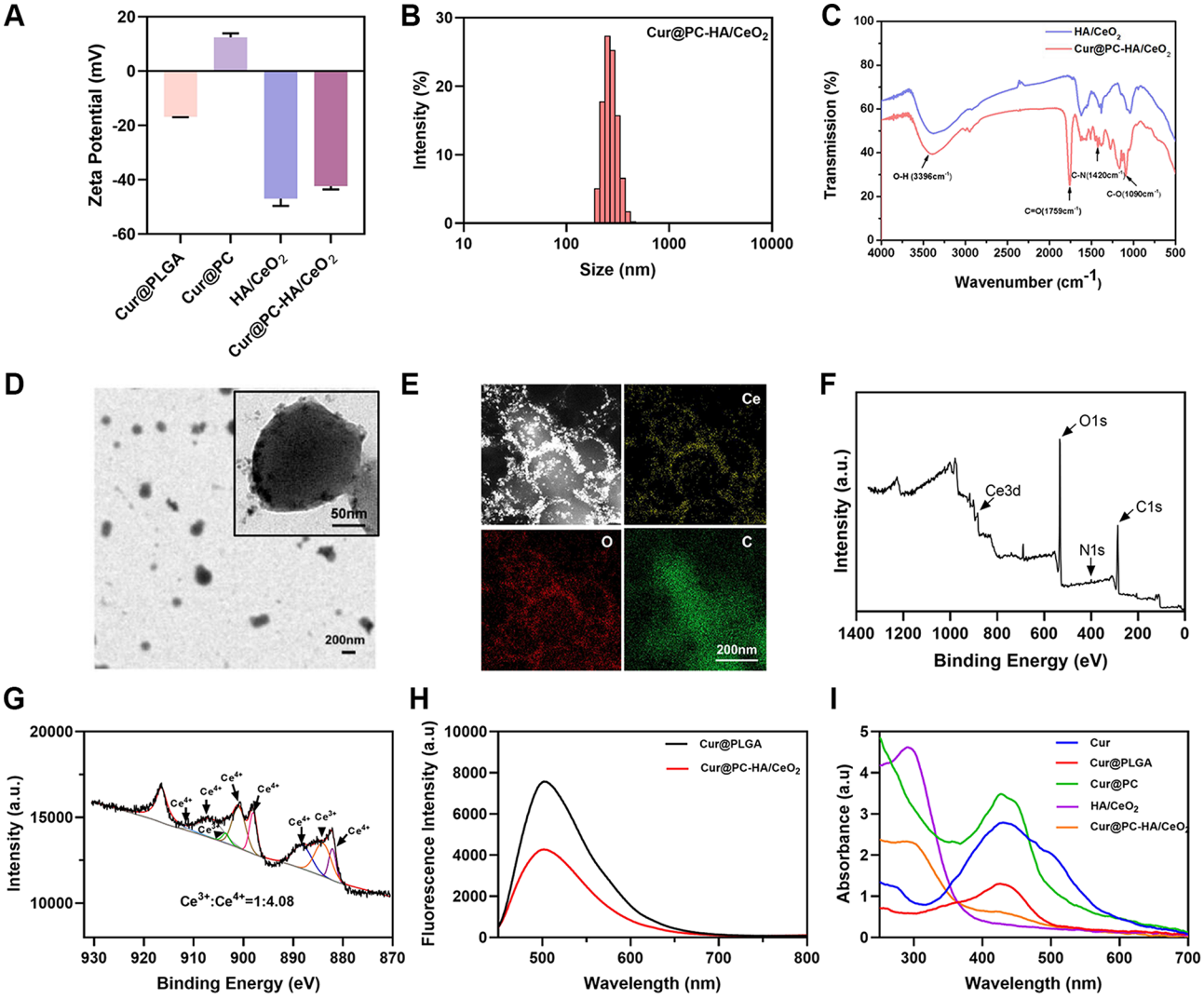

Fig. 2 Characterization of Cur@PC-HA/CeO_2NPs. (**A**) Zeta potentials of Cur@PLGA, Cur@PC, HA/CeO_2, and Cur@PC-HA/CeO_2 NPs. (**B**) DLS analysis of the size of Cur@PC-HA/CeO_2 NPs. (**C**) Fourier transform infrared spectroscopy spectra of HA/CeO_2 and Cur@PC-HA/CeO_2 NPs. (**D**) Transmission electron microscopy image of Cur@PC-HA/CeO_2 NPs. (**E**) Elemental mappings of Cur@PC-HA/CeO_2 NPs, including Ce, O, and C elements. (**F**, **G**) X-ray photoelectron spectroscopy analysis shows the chemical valence of Ce on the surface of Cur@PC-HA/CeO_2 NPs. (**H**) Fluorescence emission spectra of Cur@PLGA and Cur@PC-HA/CeO_2 NPs. (**I**) The ultraviolet-visible absorption spectra of Cur, Cur@PLGA, Cur@PC, HA/CeO_2, and Cur@PC-HA/CeO_2 NPs

(Fig. 2C), which demonstrated the formation of Cur@PC-HA/CeO_2 NPs.

The size and morphology of the obtained Cur@PC-HA/CeO_2 NPs were observed by transmission electron microscopy, which demonstrated a spherical core–shell structure (Fig. 2D) with an approximately 174 nm particle size. Furthermore, energy-dispersive X-ray analysis revealed that Ce from the HA/CeO_2 NPs was uniformly distributed on the surface of the Cur@PC core (Fig. 2E). X-ray photoelectron spectroscopy (XPS) data demonstrated the coexistence of Ce^{3+} and Ce^{4+} peaks in the spectra (Fig. 2F-G), indicating the presence of mixed Ce valence states in the resultant Cur@PC-HA/CeO_2 NPs. The Ce^{3+}/Ce^{4+} ratios for HA/CeO_2 and Cur@PC-HA/CeO_2 were 0.21 and 0.25, respectively (Fig. 2G, Additional file 1: Fig. S6), suggesting that the coupling reaction between HA/CeO_2 and Cur@PC NPs did not significantly affect the valence states of Ce. Furthermore, fluorescence spectroscopy results verified the successful encapsulation of Cur in Cur@PC-HA/CeO_2 NPs (Fig. 2H), whereas the characteristic absorption peaks of Ce (290 nm) and Cur (430 nm) appeared in the ultraviolet-visible absorption spectra of Cur@PC-HA/CeO_2 NPs (Fig. 2I). The drug-loading content and encapsulation efficiency of Cur in the obtained Cur@PC-HA/CeO_2 NPs were 15.3% and 94.5%, respectively. And the efficiencies of cerium in HA/CeO_2 NPs and Cur@PC-HA/CeO_2 NPs were 19.7% and 14.3%, respectively.

In vitro enzyme-responsive drug release

Although HA or HA-based NPs have been widely used for targeted colon inflammation or tumor treatment, the absorption of orally administered HA remains controversial [7, 31, 32]. HA with different molecular weights (MWs) may demonstrate variable metabolic processes following oral administration: HA with high molecular weight can be selectively absorbed in the large intestine, whereas the small molecules of HA scarcely reach the lower GIT owing to their non-specific absorption by natural human metabolism, such as the portal vein and lymph vessels in the gastrointestinal sites [24]. To analyze the influence of HA MWs on the stability and drug release behavior of NPs, we synthesized Cur-loaded NPs with high-MW of HA (HMW-HA, defined here as 200–400 kDa) and with low-MW of HA (LMW-HA, defined here as ≤3000 Da). As shown in Fig. 3A and Additional file 1: Fig. S7, both HMW-HA and LMW-HA NPs exhibited higher release rates of Cur under simulated colon fluids (SCF, pH 7.4, with β-glucuronidase and hyaluronidase) than under pH media, indicating the colonic enzyme responsiveness of the designed NPs. Thereafter, we compared the in vitro release profiles of Cur-loaded NPs with HMW-HA and LMW-HA in several artificial media that simulated different physiological environments of GIT according to the previous literature: (i) simulated gastric fluid (SGF, pepsin enzyme, pH 1.2) for 2 h, (ii) simulated intestinal fluid (SIF, pancreatin enzyme, pH 6.8) for 3 h, and (iii) simulated colonic fluid (SCF, β-glucuronidase and hyaluronidase, pH 7.4) for more than 24 h [22]. A total of 15.3% of Cur was released from HMW-HA NPs 5 h following sequential incubation under non-colonic conditions (SGF and SIF, Fig. 3B). Interestingly, the release rate of Cur from the HMW-HA NPs rapidly accelerated to 35.6% after treatment with SCF, which contains enzymes capable of degrading the HA and chitosan layers, further demonstrating the colonic enzyme responsiveness of the HMW-HA NPs. For LMW-HA NPs, 18.9% of Cur was released during the first 5 h under non-colonic conditions, whereas only 7.5% of Cur was released from LMW-HA NPs in the subsequent 24 h of incubation in SCF, suggesting a lack of efficient responsiveness to colon enzymes. These results indicate that high-MW HA is more suitable for preparing colon-selective drug release systems.

Thereafter, we evaluated the impact of various enzymatic media conditions (SGF, SIF, and SCF groups) on the prepared NPs by monitoring their particle size changes following incubation with simulated GIT fluids for scheduled periods. As shown in Fig. 3C, the particle size of the HMW-HA NPs demonstrated the largest change in the SCF group, followed by the SIF group, with

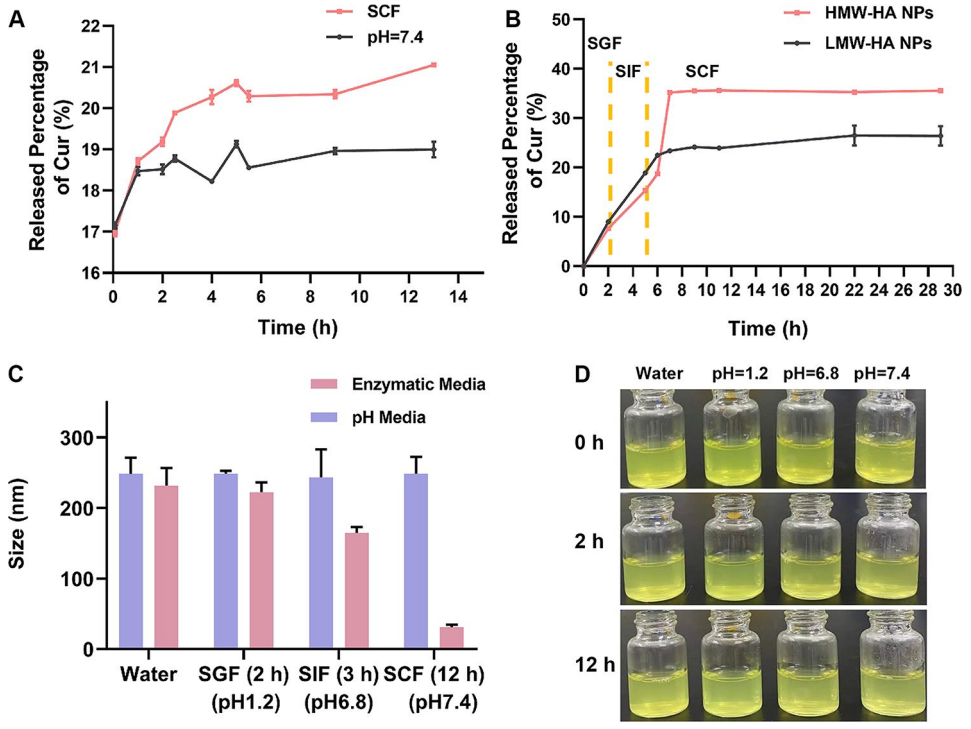

Fig. 3 In vitro drug release studies. (**A**) In vitro release kinetics of curcumin from high-molecular-weight-hyaluronic acid nanoparticles (HMW-HA NPs) under SCF and pH = 7.4 media. (**B**) In vitro release kinetics of curcumin from low molecular weight (LMW)-HA and HMW-HA NPs under simulated gastrointestinal conditions (SGF, simulated gastric fluid; SIF, simulated intestinal fluid; SCF, simulated colonic fluid). (**C**) Particle size of HMW-HA NPs when being exposed to SGF (pH 1.2) for 2 h, SIF (pH 6.8) for 3 h, and SCF (pH 7.4) for 12 h. (**D**) Photograph showing the property of HMW-HA NPs when exposed to water and different pH solutions for 0, 2, and 12 h. Data are presented as mean ± SD

no significant change in the SGF or water groups, further demonstrating their responsiveness to colonic enzymes. Meanwhile, pure pH media in the absence of enzymes did not alter the particle size or color of HMW-HA NPs (Fig. 3C-D), suggesting their great stability under acidic conditions, potentially attributable to the protective effect of HA on the particles. Taken together, the acid-resistant property and colonic enzyme-responsive drug release behavior of the prepared Cur@PC-HA/CeO_2 NPs endowed them with remarkable potential to resist the non-specific corrosion of the acidic gastric environment and release drugs in local colon areas, making them suitable for use as an oral colon-specific drug delivery system.

In vitro colitis-targeting ability and cellular uptake

An inflammatory colon cell model was used for the in vitro assays, as previously reported [33, 34]. As expected, elevated interleukin (IL)-8 expression was observed in the inflamed colon epithelial-like carcinoma cells (Caco-2, Fig. 4A), confirming the presence of inflammation in the established cell models. Furthermore, the expression level of CD44 receptor in uninflamed and inflamed Caco-2 cells were detected by fluorescence microscopy and flow cytometry. The results showed that the inflamed Caco-2 cells exhibited stronger fluorescence signal and had higher expression level of CD44 receptor than the untreated Caco-2 cells (Fig. 4B-C, Additional file 1: Fig. S8), demonstrating upregulated expression of the CD44 receptor in inflamed cells.

To investigate the targeting ability and cellular uptake of Cur@PC-HA/CeO_2 NPs through HA-CD44 receptor-mediated endocytosis, inflamed and uninflamed Caco-2 cells were treated with free Cur solution, Cur@PC NPs, and Cur@PC-HA/CeO_2 NPs (with and without 5 mg/mL HA pretreatment) for 18 h, followed by CLSM examination. As shown in Fig. 4D-E, no obvious fluorescence signals were observed in free Cur- and Cur@PC NP-treated cells, whereas a clear green fluorescence was observed in Cur@PC-HA/CeO_2 NP-treated cells. Compared with

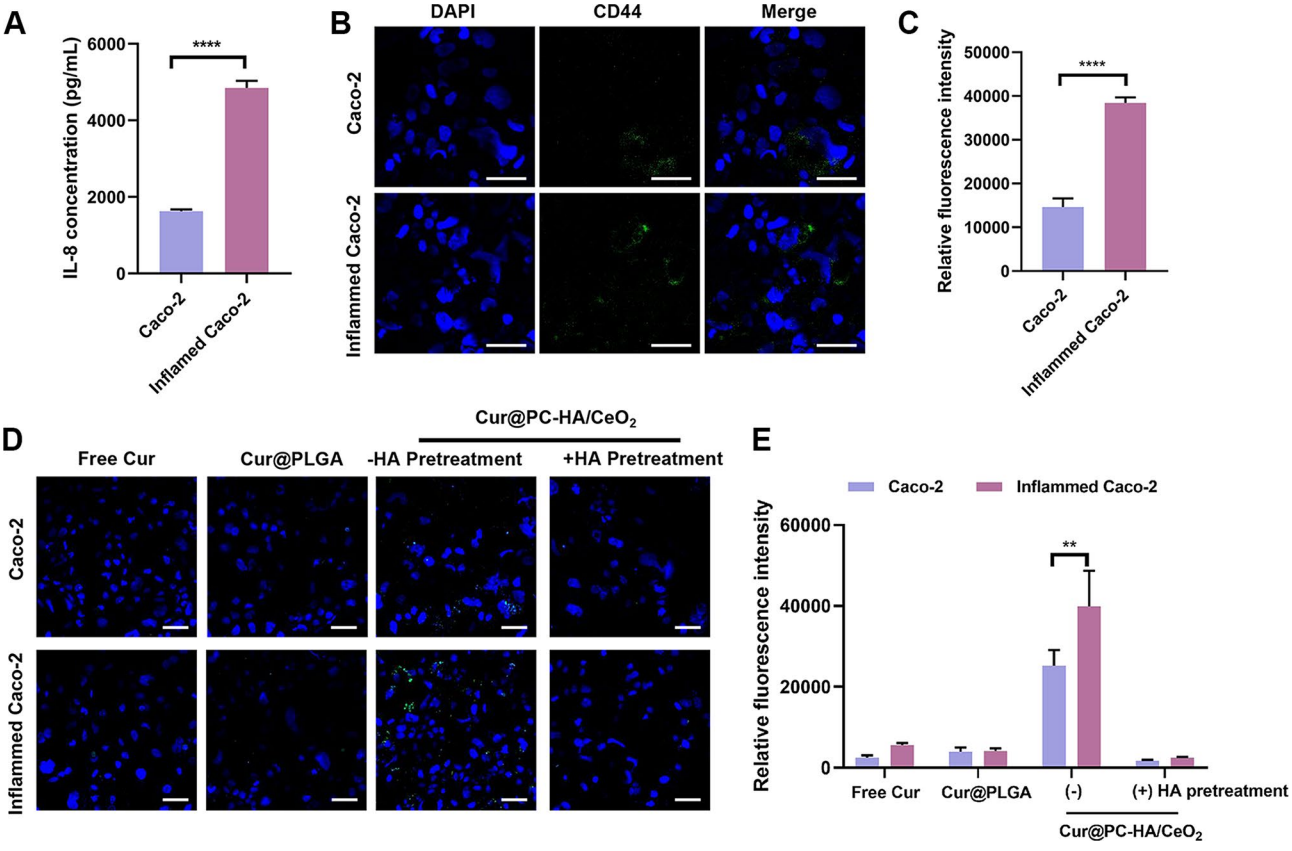

Fig. 4 Intracellular uptake study of Cur@PC-HA/CeO_2NPs in Caco-2 cells. (**A**) The levels of interleukin-8 in uninflamed and inflamed Caco-2 cells. (**B**) Confocal fluorescence images of uninflamed and inflamed Caco-2 cells. Cells were stained with CD44-labeled fluorescein isothiocyanate antibody (green) and nuclei stained with 4′,6-diamidino-2-phenylindole (blue). Scales bars, 50 μm. (**C**) The fluorescence intensity of CD44 was quantitatively analyzed using Image J software. (**D**) Confocal fluorescence images showing cellular uptake of free Cur, Cur@PLGA NPs NPs, and Cur@PC-HA/CeO_2 NPs (with or without 5 mg/mL HA pretreatment) in uninflamed and inflamed Caco-2 cells. Green and blue indicate the fluorescence of Cur and nucleus, respectively. Scales bars, 50 μm. (**E**) The fluorescence intensity of Cur in each group was quantitative analyzed using Image J software. Data are presented as mean ± SD. T-tests were performed for statistical comparison, $^{**}P < 0.01$, $^{****}P < 0.0001$

that in the uninflamed Caco-2 cells, a stronger fluorescence signal was observed in the inflamed Caco-2 cells incubated with Cur@PC-HA/CeO_2 NPs, suggesting enhanced cellular uptake by the inflamed cells. Moreover, increased cellular uptake of Cur@PC-HA/CeO_2 NPs was significantly inhibited by the pre-saturation of the CD44 receptor with excess HA. These results support the role of HA-CD44 interaction-mediated endocytosis in the targeted internalization of Cur@PC-HA/CeO_2 NPs into inflamed colon epithelial cells.

Colitis-targeting CT imaging

To investigate the X-ray attenuation property of Cur@PC-HA/CeO_2 NPs, CT imaging was performed using the commercial CT contrast agent ioversol as a control. As shown in Fig. 5A and Additional file 1: Fig. S9, the CT images of ioversol and Cur@PC-HA/CeO_2 NPs both became brighter following an increase in their concentrations, suggesting a strong X-ray attenuation effect. Similar to ioversol, Cur@PC-HA/CeO_2 NPs increased the CT signal intensity in a concentration-dependent manner (r^2=0.99) at each tube voltage (Fig. 5B, Additional file 1: Fig. S10). As expected, the CT attenuation rates (slope of the line) decreased with increasing tube voltage because the average beam energy moved further away from the K-edge of Ce (i.e., 40.4 keV). Furthermore, the CT imaging performance of Cur@PC-HA/CeO_2 NPs was superior to that of ioversol at the same concentration (Fig. 5C-D). The potential reason for this is that Ce has a slightly higher K-edge value than iodine (i.e., 33.2 keV), and therefore matches well with the clinically used X-ray beam energy [35]. These results suggest that Cur@PC-HA/CeO_2 NPs can be used as effective agents for CT imaging and produce a better contrast-enhancement effect than ioversol at a low tube voltage, which has the potential to mitigate the dosage and damage attributed to radiation exposure.

Encouraged by the strong X-ray attenuation capability of Cur@PC-HA/CeO_2 NPs in vitro, we subsequently examined the performance of Cur@PC-HA/CeO_2 NPs in noninvasive and real-time CT imaging of the GIT in living animal models. As shown in Fig. 5E, 3D-reconstructed CT images of the GIT recorded the flow of Cur@PC-HA/CeO_2 NPs throughout the entire GIT in healthy C57 mice following oral administration. At 5-min post-administration, the stomach and duodenum became bright on the CT images, indicating that the NPs had reached the proximal small intestine. After 1 h, some NPs gradually flowed into and illuminated the large intestine; 24 h later, the CT signals in the intestine became weak and even negligible, indicating that nearly all the NPs were eliminated from the GIT. Thereafter, we performed dynamic CT imaging of the lower GIT after Cur@PC-HA/CeO_2 NP administration by enema, which demonstrated substantial CT contrast enhancement in the intestine (Additional file 1: Fig.S11). These results demonstrated outstanding performance of Cur@PC-HA/CeO_2 NPs for GIT imaging in vivo.

Considering the outstanding in vitro colitis-targeting ability of the designed NPs, we subsequently investigated the potential of Cur@PC-HA/CeO_2 NPs in targeted CT imaging of colitis using a dextran sodium sulfate (DSS)-induced colitis mouse model [36]. Following oral administration, dynamic CT images of the colitis mice were recorded, showing a remarkably enhanced contrast in the GIT when the Cur@PC-HA/CeO_2 NPs passed through it (Fig. 5E-F). Such CT contrast enhancement in some large intestines can be sustained for over 24 h. However, in the ioversol group, no apparent CT signal was observed in the large intestine of colitis mice at 24 h post-administration (Fig. 5E-F). Furthermore, the large intestine with a high CT signal in the Cur@PC-HA/CeO_2 NPs group was excised and examined under electron microscopy, confirming the presence of inflammation in these areas. Quantitative analysis of Ce by inductively coupled plasma mass spectrometry (ICP-MS) demonstrated the accumulation of NPs in the inflamed tissues (Fig. 5G-H). These results indicate that Cur@PC-HA/CeO_2 NPs can be used for targeted CT imaging of colitis tissues in vivo. Interestingly, a similar colitis-targeted tracking effect of Cur@PC-HA/CeO_2 NPs was also achieved in colitis mice induced by enema (Additional file 1: Fig. S11-S12). Moreover, these NPs could accumulate in the colitis tissues for up to 24 h, indicating that the Cur@PC-HA/CeO_2 NPs could not only be used for real-time colitis-targeting imaging but also for a prolonged treatment time window.

Protective effect against oxidative damage in colitis

Multiple studies have shown that the occurrence and development of IBD was closely associated with excessive oxidative stress [37–40]. As effective nanozymes, CeO_2 NPs reportedly possess robust multiple ROS scavenging capabilities by the electron transfer between Ce^{3+} and Ce^{4+}, as well as the resultant hybrid superoxide dismutase (SOD)- and catalase (CAT)- mimetic enzyme activities [41–43]. Moreover, CeO_2 NPs possess autocatalytic capacities that enable them to easily recover their antioxidant activity and repetitively eliminate ROS [44]. XPS confirmed the presence of hybrid valence states of Ce^{3+} and Ce^{4+} in the HA/CeO_2 and Cur@PC-HA/CeO_2 NPs (Fig. 2G, Additional file 1: Fig. S6). As shown in Fig. 6A, the HA/CeO_2 solution rapidly turned yellow following the addition of hydrogen peroxide (H_2O_2). During the subsequent 10 days, the yellow solution gradually recovered its original color as H_2O_2 decomposed from the nanoparticle suspension. Meanwhile, re-addition of H_2O_2 could induce the above-mentioned color change again, thus confirming the admirable autocatalytic

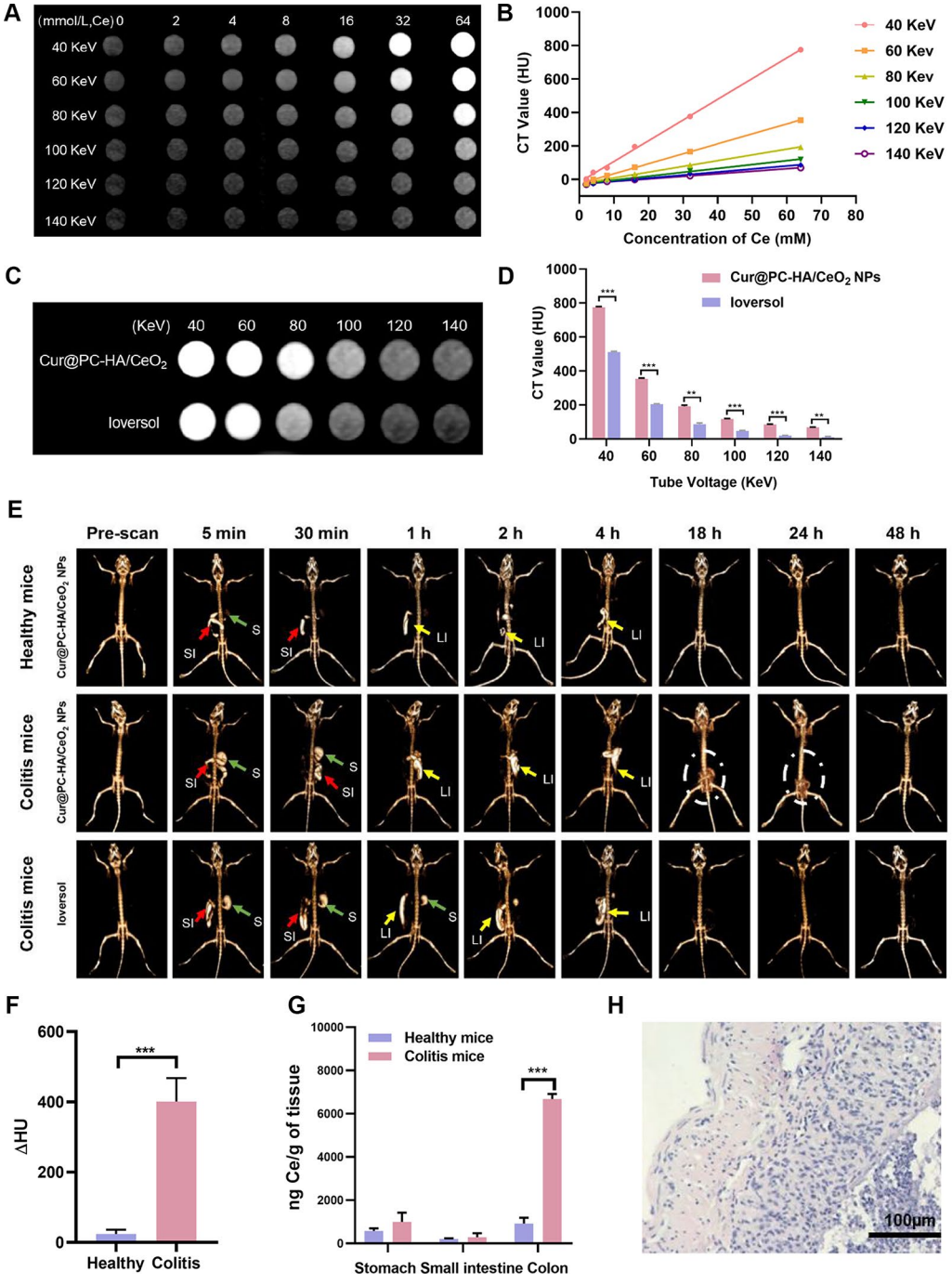

Fig. 5 In vitro X-ray attenuation property and in vivo IBD targeting computed tomography (CT) performance of Cur@PC-HA/CeO_2NPs.In vitro CT images (**A**) and corresponding linear correlations of the CT signals (**B**) with the concentrations of Cur@PC-HA/CeO_2 NPs at different tube voltages. Representative CT image (**C**) and the CT signals (**D**) of Cur@PC-HA/CeO_2 (64 mM Ce) and ioversol (64 mM I) at different tube voltages. (**E**). Representative three-dimensional-rendered CT images of healthy mice and DSS-induced colitis mice, pre- and post- administration of Cur@PC-HA/CeO_2 NPs (400 μL, 64 mM Ce) or ioversol (400 μL, 64 mM I). "S", "SI", and "LI" indicate the stomach, small intestine, and large intestine, respectively. The white dashed oval indicates Cur@PC-HA/CeO_2 NPs accumulation in the diseased areas of colitis. (**F**) The CT signal histogram in the colon of the healthy and colitis groups at 24 h following oral administration of Cur@PC-HA/CeO_2 NPs. (**G**) Ce contents in the digestive organs of mice in the healthy and colitis groups at 24 h post-administration of Cur@PC-HA/CeO_2 NPs. (**H**) Representative hematoxylin and eosin staining image of colon from colitis mice, which show high CT signals at 24 h post-administration of Cur@PC-HA/CeO_2 NPs. Scale bars, 100 μm. Data are presented as mean ± SD. T-tests were performed for statistical comparison, $^{*}P < 0.05$, $^{**}P < 0.01$, $^{***}P < 0.001$

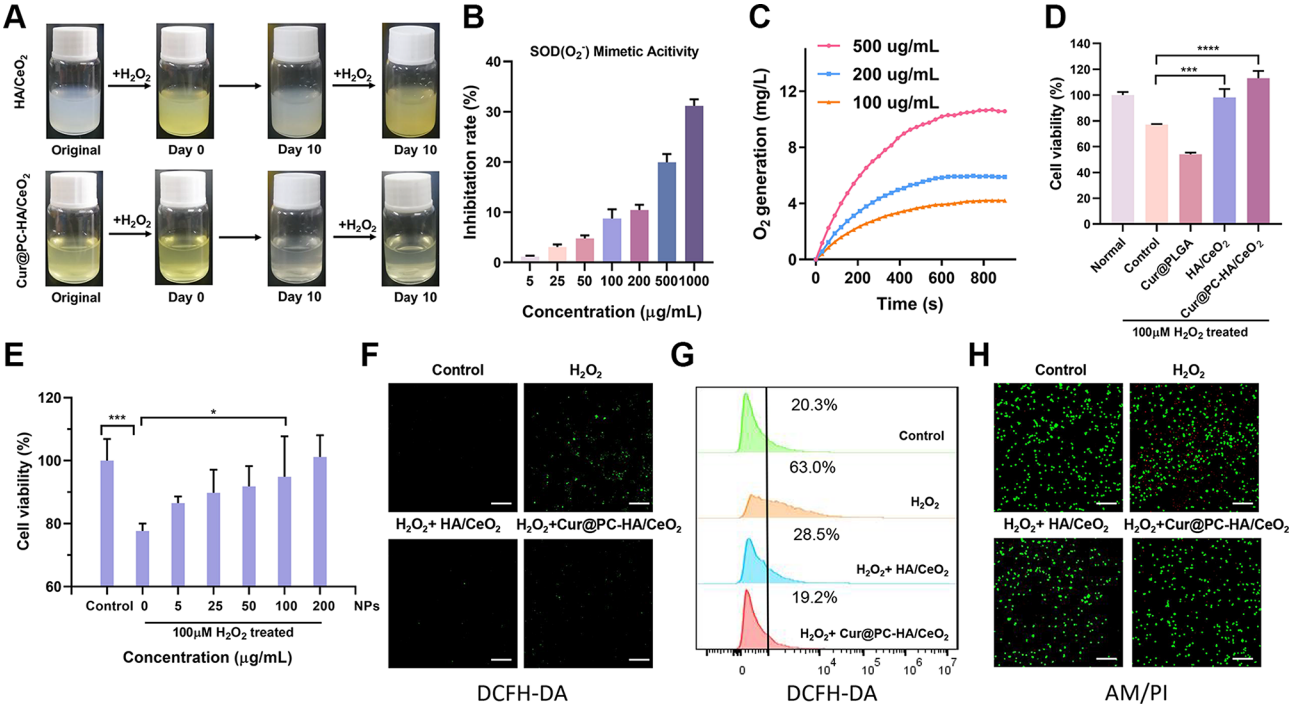

Fig. 6 Protective effect of Cur@PC-HA/CeO_2NPs against oxidative damage in vitro. (**A**) Regeneration cycle of cerium oxide (CeO_2): temporal color change in the samples indicates transition between Ce^{3+} (white) and Ce^{4+} (yellow color). (**B**) Reactive oxygen species (ROS) scavenging activity of Cur@PC-HA/CeO_2 NPs mimics superoxide dismutase (SOD). (**C**) Oxygen generation from H_2O_2 (100 μM) catalyzed by CAT-mimicking activity of Cur@PC-HA/CeO_2 NPs. (**D**) Viability of HT-29 cells following 24 h treatment with PBS, H_2O_2 (100 μM) + PBS, H_2O_2 (100 μM) + Cur@PLGA (200 μg/mL), H_2O_2 (100 μM) + hyaluronic acid (HA)/CeO_2 (200 μg/mL), or H_2O_2 + Cur@PC-HA/CeO_2 (200 μg/mL). (**E**) Viability of HT-29 cells after 24 h treatment with different concentrations of Cur@PC-HA/CeO_2 in the presence of 100 μM H_2O_2. (**F**) ROS scavenging activities in H_2O_2 stimulated Caco-2 cells were investigated by evaluating the fluorescence of DCFH-DA. (**G**) ROS scavenging activities in H_2O_2 stimulated HT-29 cells were investigated by flow cytometry. (**H**) Fluorescence imaging of HT-29 cells stained by Calcein-AM/PI following 24 h treatment with PBS, H_2O_2 (100 μM) + PBS, H_2O_2 (100 μM) + HA/CeO_2 (200 μg/mL), or H_2O_2 + Cur@PC-HA/CeO_2 (200 μg/mL). Scale bars, 200 μm. Data are presented as mean ± SD. One-way of ANOVA were performed for statistical comparison, $^*P < 0.05$, $^{**}P < 0.01$, $^{***}P < 0.001$

properties of the HA/CeO_2 NPs. Furthermore, the Cur@PC-HA/CeO_2 solution exhibited color changes similar to those of HA/CeO_2, indicating that the assembly of NPs did not affect the autocatalytic properties of the HA/CeO_2 nanozymes. In addition, the SOD-mimetic catalytic capacity of NPs was measured by enzyme-linked immunosorbent assay, demonstrating the highly sensitive and concentration-dependent scavenging activity of ROS by Cur@PC-HA/CeO_2 NPs (Fig. 6B). H_2O_2 is generated by $\cdot O_2^-$ disproportionation, which can be further decomposed into H_2O and O_2 by CAT enzyme activity. Using a dissolved oxygen meter, the CAT-mimicking activity of Cur@PC-HA/CeO_2 NPs was investigated by monitoring the catalytic decomposition of O_2 generated by H_2O_2. As shown in Fig. 6C, Cur@PC-HA/CeO_2 NPs could catalyze the production of O_2. In addition, as the concentration increased, Cur@PC-HA/CeO_2 NPs showed enhanced H_2O_2 scavenging ability.

The protective effects of different NPs against oxidative damage were explored using H_2O_2 as a toxic oxidant. Treatment with H_2O_2 alone and H_2O_2+Cur@PLGA NPs significantly lowered cell viability. However, when the cells were pretreated with HA/CeO_2 and Cur@PC-HA/CeO_2 NPs, the cell viability significantly improved, indicating that both HA/CeO_2 and Cur@PC-HA/CeO_2 NPs protected the cells from oxidative damage induced by H_2O_2 (Fig. 6D). Moreover, Cur@PC-HA/CeO_2 NPs exhibited outstanding cellular protection effects at concentrations even as low as 100 μg/mL (Fig. 6E). Then intracellular ROS scavenging activities were detected by fluorescence microscopy and flow cytometry. Satisfactorily, HA/CeO_2 and Cur@PC-HA/CeO_2 NPs treatment could reduce intracellular ROS levels significantly compared to H_2O_2-treated only (Fig. 6F-G). As shown in Fig. 6H, both HA/CeO_2 and Cur@PC-HA/CeO_2 NPs could attenuate oxidative stress-induced cell apoptosis by eliminating intracellular ROS, and the Cur@PC-HA/CeO_2 NPs had a better effect. This enhanced effect is likely due to the additional antioxidant property of Cur [18, 19]. These results demonstrate the outstanding nanozyme capability of Cur@PC-HA/CeO_2 NPs, confirming their great potential as nano-antioxidants for IBD treatment.

Theranostics of Cur@PC-HA/CeO_2 NPs for colitis in vivo

To confirm the theranostic effect of Cur@PC-HA/CeO_2 NPs in vivo, experiments were performed in DSS-induced acute colitis mice. The mice were randomly divided into five groups: healthy mice treated with water (i, the control group as the negative control), and DSS-induced colitis mice treated with water (ii, the colitis group as the positive control), free curcumin (Cur) (iii), Cur@PLGA NPs (iv), or Cur@PC-HA/CeO_2 NPs (v). According to the CT imaging results (Fig. 5E), Cur@PC-HA/CeO_2 NPs accumulated in the colitis tissues for up to 24 h and were completely excreted within 48 h. Therefore, the mice were administered the NPs once every 48 h, and the mice in the Cur@PC-HA/CeO_2 group underwent CT imaging 24 h after each administration during the entire experimental period.

Compared with the colitis group, Cur@PC-HA/CeO_2 treatment significantly protected animals against DSS-induced bodyweight loss and shortening of colon length (Fig. 7A-B and Additional file 1: Fig. S13). In contrast, mice treated with Cur or Cur@PLGA did not achieve full bodyweight recovery, and a subset of animals had shortened colon length. As shown in Fig. S14, the increased DAI in the colitis mice were modulated by Cur, Cur@

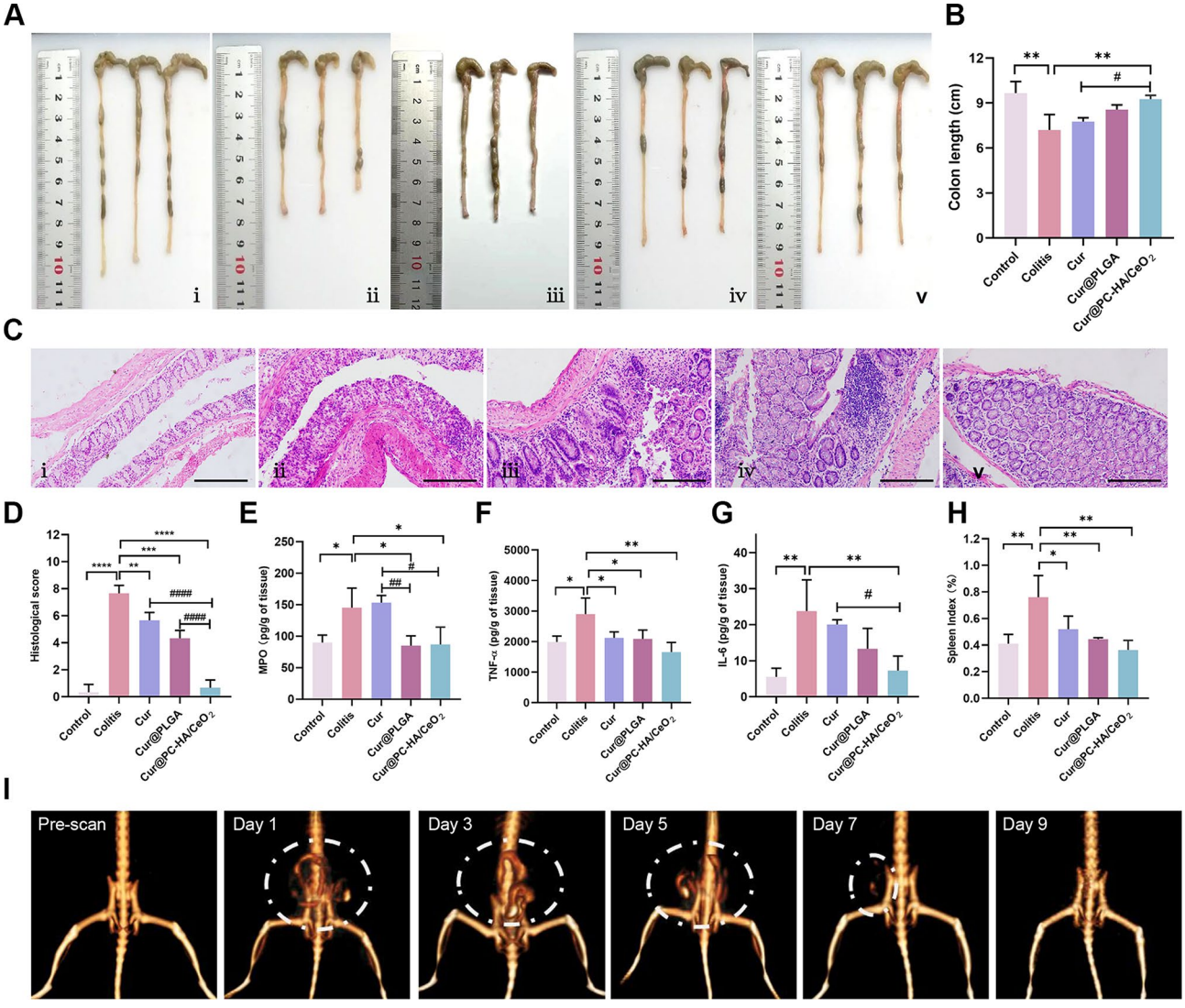

Fig. 7 In vivo IBD therapy with Cur@PC-HA/CeO_2NPs. Representative digital photos (**A**) and quantified lengths (**B**) of colonic tissues isolated from healthy or colitis mice after 10 days of different treatment (i, control; ii, colitis; iii, Cur; iv, Cur@PLGA; iv, Cur@PC-HA/CeO_2). Hematoxylin and eosin-stained histological sections (**C**) and colonic damage scores (**D**) of colon tissues. Scales bars, 200 μm. The levels of (**E**) myeloperoxidase (MPO), (**F**) tumor necrosis factor-alpha (TNF-α), and (**G**) interleukin (IL)-6 in colon tissues from healthy or colitis mice at 10 days following different treatments. (**H**) Spleen index from mice in different groups. (**I**) Representative CT images of mice in Cur@PC-HA/CeO_2 group at 24 h following oral administration during the whole treatment period. The white dashed oval indicates Cur@PC-HA/CeO_2 NPs accumulation in an area of colitis. Data are presented as mean ± SD ($n = 3$). One-way of ANOVA were performed for statistical comparison. $^{*}P < 0.05$, $^{**}P < 0.01$, $^{***}P < 0.001$, $^{****}P < 0.0001$ versus DSS-induced colitis group; $^{\#}P < 0.05$, $^{\#\#}P < 0.01$, $^{\#\#\#}P < 0.001$, $^{\#\#\#\#}P < 0.0001$ versus Cur@PC-HA/CeO_2 group

PLGA NPs and Cur@PC-HA/CeO_2 NPs. The Cur@PC-HA/CeO_2 NPs treatment evidently reversed the values to a greater extent compared to the free drug Cur and Cur@PLGA NPs.

Furthermore, hematoxylin and eosin (H&E) staining was performed to explore the inhibitory effect of Cur@HA-CeO_2 against histological damage to the colon tissue in a colitis mouse model. As expected, mice treated with DSS exhibited robust signs of inflammation, including the destruction of crypts, a decrease in the goblet cells, and inflammatory cell infiltration in the lamina propria. After treatment with Cur@HA-CeO_2 NPs, significant recovery from this pathological damage was observed, and the tissue is more closely resembled that of normal mice. In contrast, moderate recovery from pathological damage was found in the colon in the Cur sus and Cur@PLGA NPs groups (Fig. 7C-D). Intrigued by these results, we examined the impact of Cur@PC-HA/CeO_2 NPs on DSS-inflamed colonic epithelium with disrupted intestinal barrier functions. DSS-colitis mice oral administered with Cur@PC-HA/CeO_2 NPs normalized the expression patterns levels of ZO-1, tight junction-associated proteins that play pivotal roles in gut homeostasis [27]; however, other groups, including free Cur and Cur@PLGA treatment, had minimal impact on ZO-1 levels (Additional file 1: Fig. S15).

A series of studies have shown that Cur can exert anti-inflammatory effects in colitis by inhibiting NF-κB activation [45].To confirm these findings, the colonic myeloperoxidase (MPO) expression was measured as an indicator of neutrophil infiltration. MPO expression substantially increased in the colitis group, whereas this change in MPO expression was significantly reversed in both NP-treated groups (Fig. 7E). In addition, the increase in the level of pro-inflammatory cytokines, including TNF-α and IL-6, was significantly decreased by Cur@PC-HA/CeO_2 NPs treatment in the colitis mice (Fig. 7F-G). However, Cur@PLGA treatment only slightly decreased the level of these pro-inflammatory cytokines. In contrast, there was no statistically significant difference in MPO and IL-6 levels between the colitis and Cur groups. Additionally, the spleen index (the percentage of spleen-to-body weight) in each group demonstrated a trend similar to that of the pro-inflammatory cytokines (Fig. 7H). These results support that Cur@PC-HA/CeO_2 possesses a strong therapeutic efficacy against IBD, whereas Cur and Cur@PLGA NPs treatment exerted a limited effect on alleviating colonic inflammation.

Based on the aforementioned colitis-targeting CT imaging performance, we further evaluated the CT imaging-based therapy monitoring effect of Cur@HA-CeO_2 NPs on inflamed colons in vivo. 3D-reconstructed CT images of the inflamed GIT are shown in Fig. 7I. On day 1, bright signals were observed in the large intestines of colitis mice, indicating inflamed lesions of the colon. The extent of intestinal inflammation with high CT attenuation gradually diminished following multiple administrations of Cur@PC-HA/CeO_2 NPs. After treatment for four times, no obvious CT signal was detected in the large intestine of the mice 24 h post-administration of the NPs. We assumed that the intestinal inflammation in the Cur@PC-HA/CeO_2 group was relieved following multiple treatments with NPs, which could be quickly eliminated from the body instead of selectively accumulating in the intestine. As shown in Fig. 7, the GIT signal changes in the CT images of the Cur@PC-HA/CeO_2 group were consistent with the trends of other clinical indicators, which further confirmed colitis recovery. Thus, these results demonstrate that Cur@PC-HA/CeO_2 as a novel theranostic agent could achieve great anti-inflammatory therapeutic effects and simultaneously monitor the IBD therapy response in a real-time, noninvasive manner.

Intestinal microbiota modulation

It is reported that dysfunction of gut microbiota is closely associated with the occurrence and development of IBD [37, 38, 40]. Considering the regulatory role of HA and Cur in modulating the gut microbiota and immunity in enteric infections and inflammation [26, 27, 46], we further examined whether Cur@PC-HA/CeO_2 NPs treatment modulated the composition of the gut microbiota in DSS-induced colitis mice. Mice with untreated colitis were used as positive controls and normal mice without colitis were used as negative controls. The alpha diversity analysis results showed that Cur@PC-HA/CeO_2 NPs treatment significantly improved bacterial richness (observed OTU richness) and diversity (Chao1 and Shann) in DSS-colitis mice (Fig. 8A-B, Additional file 1: Fig. S16). In addition, β-diversity displayed by principal coordinate (PCoA) analysis and nonmetric multidimensional scaling (NMDS) analysis revealed that the difference in the composition of the intestinal microbiota in the Cur@PC-HA/CeO_2 treated-group was more similar to that of the control mice, whereas the intestinal microbiota in the colitis mice were completely different from that of the normal control (Fig. 8C, Additional file 1: Fig. S17). Consistent with a previous report, a shift in the intestinal microbiota was observed in colitis mice, including reduced abundance of *Firmicutes* and increased abundances of *Bacteroidota* and *Proteobacteria* (Fig. 8D) [47]. Further analysis at the genus level demonstrated that feeding mice with DSS resulted in increased abundance of *Bacteroidetes* (known for their negative roles in both IBD animal models [48–50] and patients with IBD [51, 52]) and conditional pathogenic bacteria *Alistipes*, whereas the abundance significantly decreased following treatment with Cur@PC-HA/CeO_2 NPs (Fig. 8E-F). Notably, Cur@PC-HA/CeO_2 NPs treatment

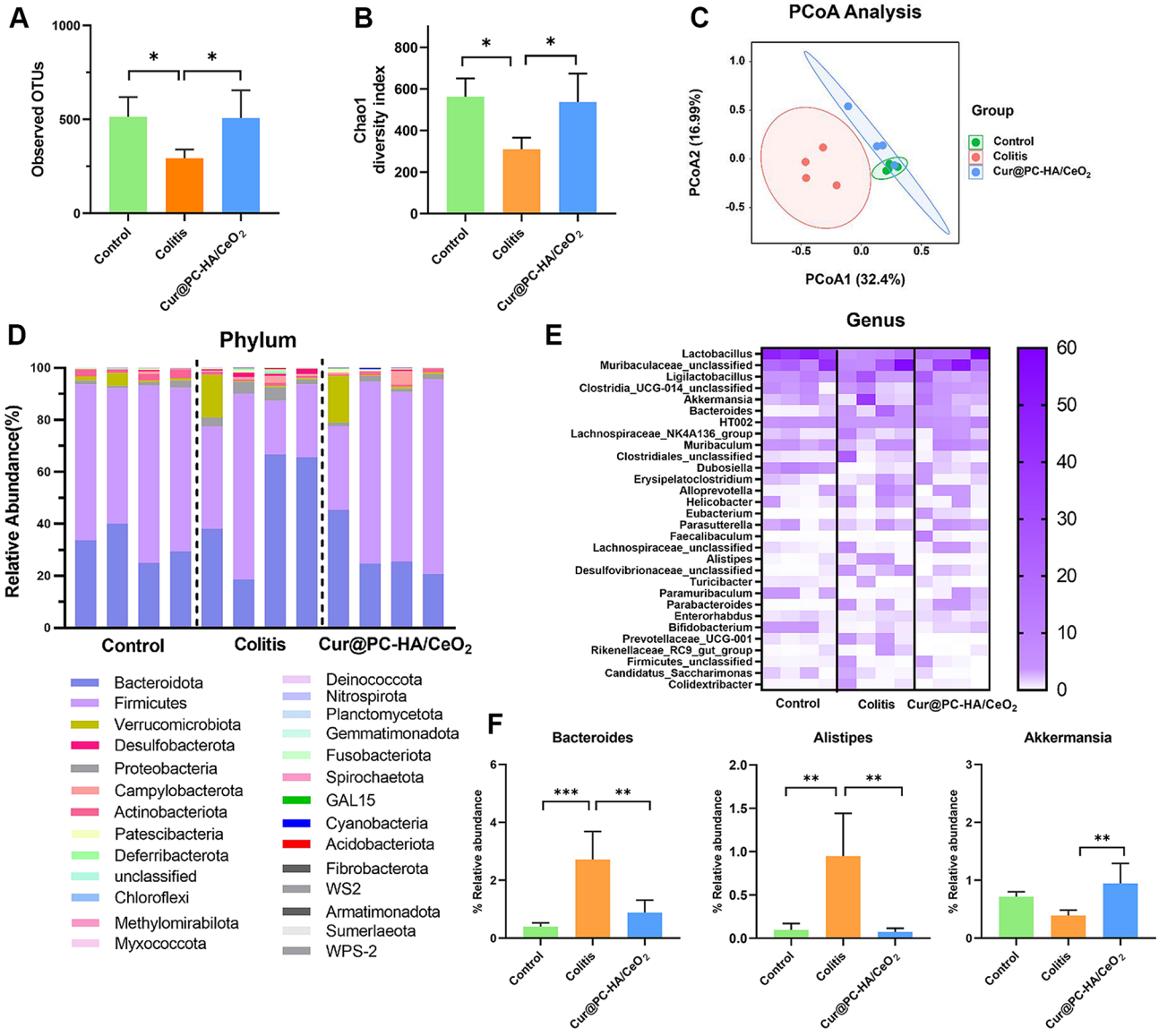

Fig. 8 Cur@PC-HA/CeO_2NPs improved the composition of gut microbiota in colitis mice. Gut microbiota α diversity measured by observed OTU (operational taxonomic unit) richness (**A**) and Chao1 diversity index(**B**). (**C**) Multiple sample principal coordinate (PCoA) analysis of microbial species abundance using the different treatment as grouping variable, based on the Bray–Curtis distance. (**D**) Relative abundance of gut microbiome. Phylum level taxonomy is presented as a percentage of the total sequences. (**E**) Heatmap displaying the relative abundance of genus-level taxa (rows) for each mouse (columns). The abundance is shown as relative percentage. (**F**) Relative abundance of selected taxa at the genus level, data are presented as mean ± SD ($n = 4$). One-way of ANOVA were performed for statistical comparison. $^{*}P < 0.05$, $^{**}P < 0.01$, $^{***}P < 0.001$

significantly increased the relative abundance of *Akkermansia* (known to be associated with protective intestinal barrier functions [53]) and *Lactobacillus* (known to have beneficial roles in both IBD animal models [48–50] and patients with IBD [51, 52]) in colitis mice (Fig. 8E-F, Additional file 1: Fig. S18). These findings indicate that Cur@PC-HA/CeO_2 NPs greatly improved the composition of the intestinal microbiota in colitis mice.

Biocompatibility of Cur@PC-HA/CeO_2 NPs

In vitro and in vivo toxicity are critical concerns for the biomedical applications of nanomaterials. First, the cytotoxicity of Cur@PC-HA/CeO_2 and HA/CeO_2 NPs was assessed in human colon epithelial-like carcinoma cells (HT-29) using an MTT assay. As presented in Additional file 1: Fig. S19-S20, viability of HT-29 cells remained over 80% following exposure to HA/CeO_2 and Cur@PC-HA/CeO_2 NPs at various concentrations, even up to 500 μg/mL, for 24 h, indicating good biocompatibility of HA/CeO_2 and Cur@PC-HA/CeO_2 NPs in vitro. Thereafter,

we investigated the in vivo toxicity of the oral administration of PBS or PBS containing Cur@PC-HA/CeO_2 NPs to C57BL/6 mice for 1 day or 14 days. After euthanization, blood and organ samples were collected for further examination and histological analyses. As shown in Fig. 9A and Additional file 1: Fig. S21, H&E staining images of the digestive and other major organs (heart, liver, spleen, lung, and kidney) in the 1-day or 14-days groups were not significantly different from those of the control group. Moreover, no significant differences were observed in routine blood biochemical indices between the control and 1-day or 14-days groups (Fig. 9B-C), further demonstrating the favorable compatibility of Cur@PC-HA/CeO_2 NPs in vivo.

Thereafter, we evaluated the metabolism and clearance of Cur@PC-HA/CeO_2 NPs in healthy C57BL/6 mice upon quantitative analysis of the Ce content in the major organs at 24 h following the oral administration of Cur@PC-HA/CeO_2 NPs, with deionized water as the control. ICP-MS analysis (Fig. 9D) demonstrated that Cur@PC-HA/CeO_2 NPs were completely eliminated from the body over 24 h, consistent with the CT images (Fig. 5E). The rapid clearance of Cur@PC-HA/CeO_2 NPs is beneficial for further clinical translation.

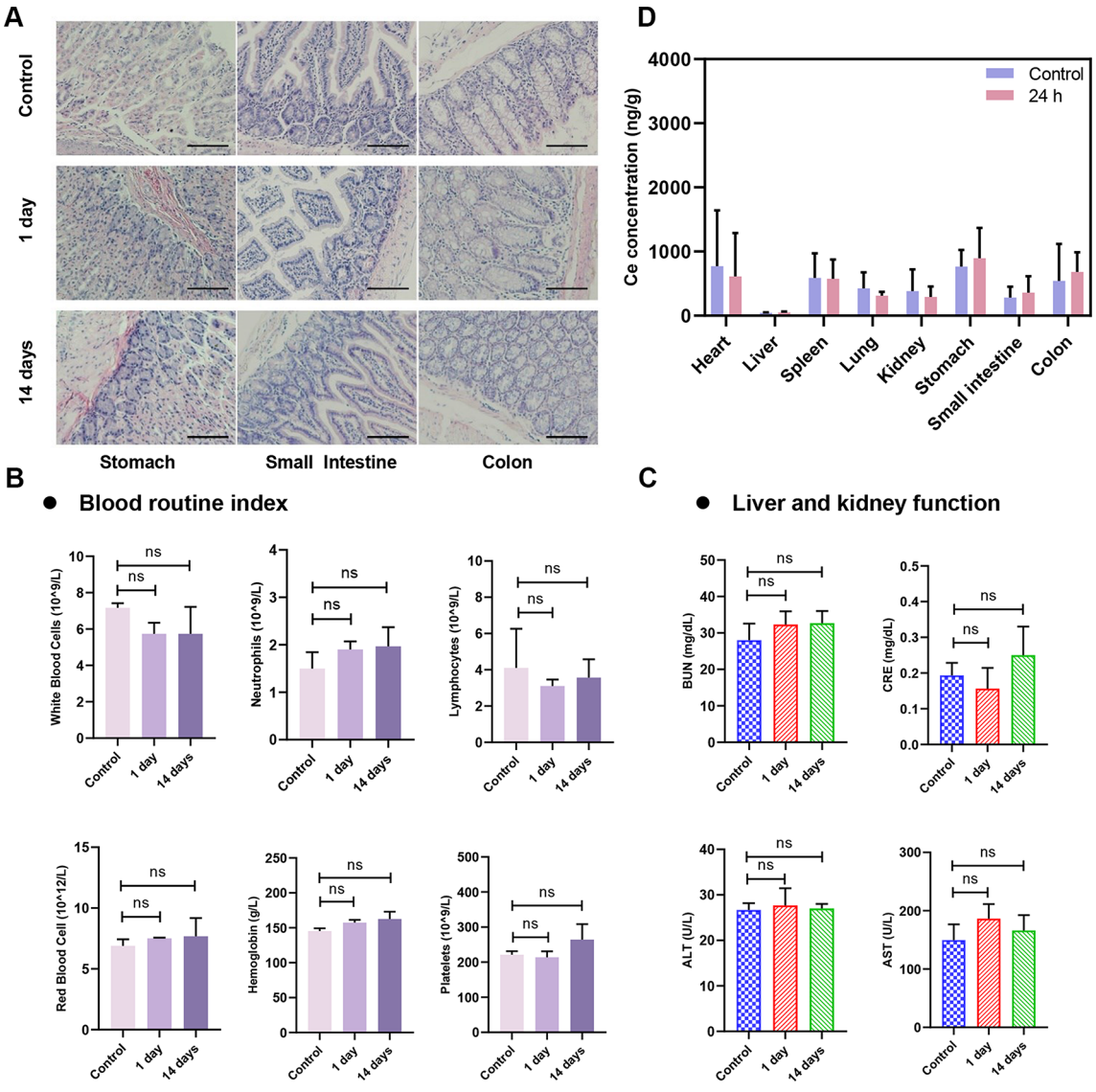

Fig. 9 In vivo biodistribution and biosafety of Cur@PC-HA/CeO_2NPs. Hematoxylin and eosin-stained histological sections of the digestive organs (**A**), blood routine indexes (**B**), and liver/kidney functions (**C**) at 1-day or 14-days post-administration of Cur@PC-HA/CeO_2 NPs in C57BL/6 mice, including blood urea nitrogen (BUN), creatinine (CRE), alanine transaminase (ALT), and aspartate transaminase (AST). Scales bars, 100 μm. (**D**) Inductively coupled plasma mass spectrometry analysis of Ce contents in various organs of C57BL/6 mice at 1 day following oral administration of Cur@PC-HA/CeO_2 NPs. Healthy C57BL/6 mice treated with PBS served as a control. Data are presented as mean ± SD ($n = 3$). One-way of ANOVA were performed for statistical comparison. ns indicates no significant difference

Conclusion

We successfully developed novel theranostic oral delivery NPs for targeted CT imaging, therapy, and colitis monitoring. Cur@PC-HA/CeO_2 NPs demonstrated impressive properties including gastrointestinal stability, colitis-targeting ability, and CT-visualized theranostic and protective effects against intestinal inflammation. In vivo and in vitro studies demonstrated that such NPs can efficiently accumulate in colitis tissues via HA receptor-mediated active targeting. Following oral administration into DSS-induced colitis mice, Cur@PC-HA/CeO_2 NPs achieved targeted CT imaging of the inflamed colon and remarkable relief in the colitis symptoms. The great therapeutic effect of Cur@PC-HA/CeO_2 NPs was attributed to the synergistic effect of its nanozyme function and intestinal microbiota regulation ability. The therapeutic efficacy can be monitored using CT imaging in a real-time and non-invasive manner. Moreover, the prepared NPs are easily cleared from the body, demonstrating outstanding biosafety. In summary, our study provides a proof-of-concept for the design and application of a novel theranostic integration strategy for simultaneous real-time diagnosis and treatment of IBD, which is a promising approach for the effective and personalized management of IBD.

Materials and methods

Materials

Hyaluronate (HA, BR, 97%) and poly(vinyl alcohol) (PVA, average Mw ~ 27,000) were purchased from RHAWN Reagent Co., Ltd.(Shanghai, China). Dulbecco's modified Eagle medium (DMEM) and fetal bovine serum (FBS) were obtained from Solarbio (Beijing, China). PLGA (Mw = 38–54 kg/mol), chitosan (high viscosity, >400 mPa.s), N-hydroxy succinimide (NHS), 1-(3-dimethylaminopropyl)-3-ethylcarbodiimide hydrochloride (EDC), cerium chloride heptahydrate ($CeCl_3{\cdot}7H_2O$), 3-(4,5-Dimethylthiazol-2-yl)-2,5-diphenyl tetrazolium bromide assay (MTT), calcein-acetoxymethyl ester (calcein-AM), propidium iodide (PI), 2',7'-dichlorodihydrofluorescein diacetate (DCFH-DA), and dextran sulfate sodium salt (DSS, MW 40000) were supplied by Aladdin Reagent Co. Ltd. (Shanghai, China). All commercial products were used without further purification.

Synthesis of HA/CeO_2 nanoparticles

HA/CeO_2 nanoparticles were synthesized following a previously reported procedure with some modifications [54]. Generally, the HA/CeO_2 nanoenzymes were formed via precipitation of cerium salts after addition to concentrated ammonia in the presence of HA polysaccharide. In brief, 200 μL of 0.7 mol/L $CeCl_3{\cdot}7H_2O$ was added to 4 mL of 2.5 mg/mL HA solution and stirred for 30 min. Then, 100 μL of concentrated ammonia was slowly added and stirred until the solution turned pale yellow. The product was dialyzed for 24 h, washed with deionized (DI) water three times at 12,000 rpm, and stored at 4 °C for future use.

Fabrication of curcumin loaded PLGA nanoparticles

Briefly, 4 mg curcumin and 80 mg PLGA were dissolved in 2 mL of dichloromethane (DCM)-methanol co-solvent (8:2). The mixture was then added to 10 mL of 1% PVA solution and sonicated with a probe in an ice bath (5 min, pulse on/off: 8 s/2 s, amplitude 50%). After complete stirring, the organic phase was removed using a rotary evaporator. The resulting product was collected by centrifugation at 12,000 rpm for 20 min, and washed thrice with DI water. For chitosan coating, 0.2% chitosan and 1% PVA were added to the uncoated Cur@PLGA NP pellet. The mixture was stirred for 4–6 h, followed by centrifugation at 12,000 rpm for 20 min. This process was repeated three times.

Preparation of cur@PC-HA/CeO_2 nanoprobes

To fabricate Cur@PC-HA/CeO_2 NPs, we added DMTMM into the HA/CeO_2 NPs solution and stirred it for 1 h at 37 °C to activate the carboxylic acid (-COOH) group of HA. Next, we added 1 mL of Cur@PC NPs solution into the mixture and stirred the reaction overnight. This allowed the -COOH groups of HA to covalently conjugate with the -NH_2 groups of the chitosan coating on the surface of Cur@PC NPs. After completion, the prepared Cur@PC-HA/CeO_2 NPs were dialyzed in DI water for two days to remove impurities. The product was then collected by high-speed centrifugation at 12,000 rpm and stored at 4 °C.

Characterization

The hydrodynamic diameters were characterized using a BT-90 Nanoparticle Analyzer (Better, China), and the zeta potentials were recorded using a Zetasizer Nano-series instrument (Nano ZS90, Malvern). Transmission electron microscopy (TEM) images were observed with an HT7icr700 electron microscope, and elemental mappings were acquired on a JEM-F200 electron microscope at an acceleration voltage of 200 kV. The absorption spectra of different materials were collected on a UV-vis-NIR spectrophotometer (Hitachi UV-3600 plus, Japan). Fourier transform infrared (FT-IR) spectra were recorded on a Nicolet iS10 FT-IR spectrometer (Thermo Scientific, USA). The fluorescence absorption spectra were collected using a fluorescence spectrophotometer (SHIMANZU RF-6000). Quantitative analysis of the elements was performed by inductively coupled plasma mass spectrometry (ICP-MS) (Spectro Genesis, Germany). The fluorescence images of cells after various treatments were obtained using a confocal microscopy (FV1000, Olympus, Tokyo, Japan).

Assessment of encapsulation and loading efficacy

During the preparation of Cur@PC-HA/CeO_2 NPs, the percentages of curcumin encapsulated and loaded were determined using the centrifugation method. The amount of curcumin encapsulated in the nanoparticles was measured by quantifying the free drug content in the supernatant after centrifugation at 12,000 rpm for 30 min, and then analyzed at 504 nm using fluorescence spectroscopy. The encapsulation and loading efficiency of curcumin were calculated according to the following formula:

$$\%\ Encapsulation\ efficiency = \frac{total\ mass\ of\ added\ drug - unencapsulated\ drug}{total\ mass\ of\ added\ drug} \times 100\%$$

$$\%\ Loading\ efficiency = \frac{the\ weight\ of\ drug\ loaded\ in\ nanoparticles}{the\ weight\ of\ nanoparticles\ solid\ mass} \times 100\%$$

In vitro drug release studies in simulated GI fluids

The efficacy of Cur@PC-HA/CeO_2 NPs in targeting and drug release in the colon was evaluated using an in vitro release assay that simulates gastrointestinal conditions. The NPs were sequentially incubated in simulated gastric fluid (SGF) for 2 h, simulated intestinal fluid (SIF) for 3 h, and simulated colonic fluid (SCF) for 24 h to mimic the conditions in the gastrointestinal tract (GI). SGF (pH 1.2, pepsin 0.32%, w/v) and SIF (pH 6.8, pancreatin 1%, w/v) were prepared according to United State Pharmacopoeia 25 NF 20 guidelines, while SCF comprised 0.1 M potassium phosphate buffer (pH 7.4), hyaluronidase 20 U/mL, and β-glucuronidase 20 U/mL.

At predetermined time intervals, 1 mL samples were taken from the release profile medium and centrifuged at 11,000 rpm for 5 min. The precipitate was then supplemented with 1 mL fresh simulation fluid and returned to the simulation system. The cumulative drug release from the supernatant was quantified by photometric analysis at 530 nm using a fluorescence spectrophotometer.

Inflamed intestinal barrier model

In brief, the Caco-2 cells were exposed to pro-inflammatory cytokines composed of IL-1β and LPS at 100 ng/mL and 2000 ng/mLconcentrations, respectively, for 24 h at 37 °C to induce inflammation. The untreated Caco-2 cells served as a control. To demonstrate the induction of inflammation in the cell model, we collected the extracellular media and assayed the expression levels of IL-8 using a sandwich enzyme-linked immunosorbent assay (ELISA).

CD44 receptor expression analysis

Confocal laser scanning microscopy (CLSM) was used to determine the CD44 levels on the cell surface using FITC Mouse Anti-Human CD44 antibodies (cat. no. 555478, 1: 100, BD Biosciences). Inflamed and untreated Caco-2 cells were fixed with a 4% paraformaldehyde solution for 20 min at 4 ℃, followed by overnight incubation with FITC-labeled anti-CD44 monoclonal antibodies (green fluorescence) at 4 ℃ in the dark to mark the cells. Subsequently, the cells were stained with DAPI (1 μg/mL) for 5 min. After treatment with an anti-fluorescence quenching agent, the CD44 expression levels of the cells were observed using CLSM.

In vitro cellular uptake

The cellular uptake capacity of Cur@PC-HA/CeO_2 NPs was evaluated using CLSM. Normal uninflamed Caco-2 cells and inflamed Caco-2 cells (5×10^4/well) were plated into glass petri dishes and cultured in the medium for 24 h. After removing the medium, serum-free medium with different treatments was added for 12 h, i) free-Cur solution; ii) Cur@PC NPs; iii) Cur@PC-HA/CeO2 NPs; iv) Cur@PC-HA/CeO_2 NPs with free HA (5 mg/mL) pretreatment for 1 h. After the 12 h uptake, the cells were washed three times with cold PBS, fixed with 4% paraformaldehyde for 20 min, and stained with DAPI (1 μg/mL) for 5 min to visualize the cell nuclei. Subsequently, CLSM was performed to observe and analyze the fluorescent signals in inflamed and untreated Caco-2 cells.

MTT assay

A standard MTT assay was utilized to determine the cytotoxicity of HA/CeO_2 and Cur@PC-HA/CeO_2 NPs. Initially, HT-29 cells (5,000 cells/well) were seeded in 96-well microplates with 200 μL of DMEM culture medium and allowed to attach overnight. After 24 h, the original culture medium was replaced with different final concentrations of HA/CeO2 NPs (0, 5, 10, 20, 50, 100, 200, and 500 μg/mL) or Cur@PC-HA/CeO_2 NPs (0, 10, 20, 50, 100, 200, and 500 μg/mL) and incubated for another 24 h in 5% CO_2 at 37 °C. Thereafter, the culture media were removed and each well was filled with 200 μL of fresh culture media containing MTT (5 mg/mL) followed by incubation for 2 h. The media was then discarded, and DMSO (150 μL) was added to each well. The absorbance was measured at 490 nm using a spectrophotometer. Cell viability, defined as the relative absorbance on each sample compared to that of the control, was calculated and expressed as percentage.

To evaluate the cell protection of different nanoparticles against H_2O_2-induced cytotoxicity, HT-29 cells were seeded in 96-well plates at a density of 5000 cells per well and incubated for 24 h with various nanoparticles (200 μg/mL) or different concentrations of Cur@PC-HA/

CeO_2 NPs in the presence of H_2O_2 (100 μM). Subsequently, the cell viability was assessed using the standard MTT assay, following a similar procedure as mentioned above.

Detection of reactive oxygen species (ROS)

To measure intracellular ROS generation, we utilized the oxidation of DCFH-DA. Briefly, Caco-2 or HT-29 cells (5×10^4/well) were plated into glass confocal petri dishes and allowed to attach for 24 h. Then, cells were incubated with PBS, HA/CeO_2 NPs (200 μg/mL), or Cur@PC-HA/CeO_2 NPs (200 μg/mL) in the presence of 100 μM H_2O_2 for 24 h. Cells without any treatment served as the negative control group. Subsequently, DCFH-DA (10 μM) was incubated with the cells for 30 min and washed several times with PBS, and then fluorescence images were obtained under an inverted microscope at the wavelength of 488 nm. Alternatively, the cells were washed with PBS and collected for detection by flow cytometry.

DSS-induced colitis mice model and experimental protocol

Acute ulcerative colitis in mice was induced using a published protocol [55]. In brief, female C57BL/6 mice weighing 18–25 g were treated with drinking water containing 3% (w/v) DSS (MW 40000) for 7 days to induce colitis. After colitis induction, the DSS water was replaced with regular water, and the drug treatment was initiated. The mice were divided into five groups ($n=3$): untreated healthy control group, PBS-treated colitis group, free Cur-treated colitis group, Cur@PLGA NPs-treated colitis group, and Cur@PC-HA/CeO_2 NPs-treated colitis group. The NPs-treated groups received an equal dose of curcumin (15 mg/kg) via oral gavage every 48 h for 10 days. Mice in the Cur@PC-HA/CeO_2 group received CT imaging 24 h post-administration during the treatment period. On the 10th day, the mice were sacrificed, and body weight, spleen weight, and colon length were measured. Colonic tissue homogenates were prepared, and the concentrations of MPO, TNF-α, and IL-6 were quantitated using ELISA kits according to the instructions. All animal experiments were conducted following the Guidelines for Care and Use of Laboratory Animals of the Tianjin University of Traditional Chinese Medicine of China and were approved by the Animal Ethics Committee of the Tianjin University of Traditional Chinese Medicine (TCM-LAEC2023041).

Assessment of the disease activity index

During the whole period of treatment, changes in the body weight, visible stool consistency, and fecal bleeding were assessed each day. Disease activity index (DAI) is the combined scores of weight loss, stool consistency and bleeding divided by three. Stool consistency index was determined as follows(0: normal; 1, loose stool; 2, mild diarrhea; 3, diarrhea; 4, gross diarrhea), fecal bleeding index was assessed according to the following criteria (0: none; 1:Occult bleeding in stool; 2: blood traced in stool visible; 3,obvious blood in stool; 4: totally rectal bleeding), and weight loss index was determined as follows (0: no change; 1: ≤5%; 2: 6–10%; 3: 11–20%; 4: ≥20%) [56].

CT scan procedure

To investigate CT imaging ability, both Cur@PC-HA/CeO_2 NPs and Ioverol solutions with equivalent element (Ce or I) concentrations (0, 2, 4, 6, 8, 16, 32, and 64 mM) were added respectively to 2 mL centrifuge tubes. These tubes were securely placed in a plastic tube rack, and CT scanning was conducted using a clinical spectral CT scanner (Siemens SOMATOM Definition Edge). Imaging parameters included a 250 ms rotation time, adaptive tube current, and tube voltage of 80/140 keV. Data obtained from the scans was transferred to the Syngo Acquisition Workplace post-processing workstation, and virtual monochromatic images were reconstructed within the photon energies range of 40–140 keV, with a 20-keV increment.

In vivo CT imaging

In vivo imaging experiments were performed with a clinical spectral CT scanner (Siemens SOMATOM Definition Edge). CT images were acquired using the following parameters, slice thickness 0.6 mm, 330 ms rotation time, adaptive tube current, and tube voltage of 80 KeV and iterative reconstruction kernel. The DSS-induced acute colitis mouse model was established to explore the CT imaging ability of Cur@PC-HA/CeO_2 in vivo. In brief, mice with or without colitis were divided into three groups: Healthy mice without colitis administered with Cur@PC-HA/CeO_2 NPs; Colitis mice administered with Cur@PC-HA/CeO_2 NPs; Colitis mice administered with Ioverol. All mice were scanned with CT, and then the mice were gavaged with either Cur@PC-HA/CeO_2 NPs or Ioverol at an equivalent element concentrations (400 μL, 64 mM Ce or I). After administration, in vivo CT imaging was performed at 5 min, 30 min, 1 h, 2 h, 4 h, 18 h, 24 h and 48 h. And the obtained CT images were subjected to 3D reconstruction analysis (Amira 4.1.2). Such areas of the large intestine where CT contrast enhancement can last for more than 24 h, colonic inflammation has been confirmed by pathological sections. And the deposition of Ce within Cur@PC-HA/CeO_2 NPs in large intestine tissue was further validated by ICP-MS. The CT values of the large intestine region in mice at 24 h after administration with Cur@PC-HA/CeO_2 NPs were recorded from three different slices and averaged.

Biosafety assessment

To assess the in vivo biocompatibility of Cur@PC-HA/CeO_2 NPs, healthy C57BL/6 mice were orally administered with either PBS or PBS containing Cur@PC-HA/CeO_2 NPs (400 μL, 5 mg/mL, 64 mM Ce) for 1 day and 14 days. After euthanizing the mice, organ samples were collected and some were subjected to H&E staining for histological evaluation. The remaining organ samples were weighed and dissolved in concentrated nitric acid solution, and the amount of Ce elements in different samples was analyzed using ICP-MS. Additionally, blood samples were collected for hematological and biochemical analysis prior to euthanization of the animals.

Histology analysis

Tissue samples were fixed in 10% neutral buffered formalin for more than 24 h, and then dehydrated with ethanol. After dehydration, tissue samples were embedded in paraffin, sectioned (5 μm), and then stained with hematoxylin and eosin (H&E). After staining, images were observed by a Nikon ECLIPSE TI-SR (Tokyo, Japan) fluorescence microscope. The severity of colonic histological damage was scored in a blinded fashion to prevent observer bias, as previously described [57].Briefly, colonic damage was assigned scores as follows: for the epithelium (E), the standards are as follows: 0, normal morphology; 1, loss of goblet cells; 2, loss of goblet cells in large areas; 3, loss of crypts; and 4, loss of crypts in large areas. For the infiltration (I), it was evaluated by the following standard scores: 0, no infiltrate; 1, infiltrate around the crypt basis; 2, infiltrate reaching the muscularis mucosae; 3, extensive infiltration reaching the muscularis mucosae and thickening of the mucosa with abundant edema; and 4, infiltration of the submucosa. The total histological score was presented as E+I.

Immunofluorescence staining

Colonic tissue sections were deparaffinized and rehydrated with xylene, 100% and 95% ethanol, and antigen retrieved through a heat-induced antigen retrieval method in 10 mM sodium citrate buffer (pH 6.0). The slides were then blocked with 10% goat serum for 30 min at 37 °C and incubated with primary antibodies as follows: ZO-1 rabbit polyclonal antibody (cat. no. 61-7300, 1:100, Invitrogen) together overnight at 4 °C. The second antibody against mouse was conjugated with anti-rabbit antibody with Alexa fluor-488 for 1 h at 37 °C. Nuclei were counterstained with DAPI for 3 min. Images were captured using a fluorescence microscope (Fluoview FV1000, Olymups, Japan).

Gut microbiota analysis

The gut microbiota analysis of Cur@PC-HA/CeO_2 NPs was evaluated in mice after a 10-day treatment. Acute ulcerative colitis in female C57BL/6 mice was induced as mentioned above, after colitis induction, the mice were divided into three groups (n=4): untreated healthy control group, PBS-treated colitis group and Cur@PC-HA/CeO_2 NPs-treated colitis group. The Cur@PC-HA/CeO_2 NPs treated groups received an equal dose of curcumin (15 mg/kg) via oral gavage every 48 h for 10 days. On the last day of the experiment, 3 pellets of feces per mouse were collected and added into EP tube.These fece samples were properly packaged and shipped to the Lianchuan Biotechnology Co., Ltd(Hangzhou, China) and all the processes showed in the below were performed by the Lianchuan Biotechnology Co., Ltd(Hangzhou, China).

Total DNA was extracted from fecal samples using the E.Z.N.A. ®Stool DNA Kit (D4015, Omega, Inc., USA) according to manufacturer 's instructions. The V3-V4 regions of 16 S rRNA genes were amplified using the universal primers 341 F (5'-CCTACGGGNGGCWGCAG-3') and 805R (5'-GACTACHVGGGTATCTAATCC-3') [58]. PCR amplification was performed with 25 ng of template DNA, 12.5 μL PCR Premix, 2.5 μL of each primer, and PCR-grade water in a total volume of 25 μL. The PCR conditions included an initial denaturation at 98 °C for 30 s, followed by 32 cycles of denaturation at 98 °C for 10 s, 54 °C for 30 s and extension at 72 °C for 45 s. The final extension step was performed at 72 °C for 10 min. The PCR products were confirmed with 2% agarose gel electrophoresis. The PCR products were purified by AMPure XT beads (Beckman Coulter Genomics, Danvers, MA, USA) and quantified by Qubit (Invitrogen, USA). The completed library was sequenced using the Illumina NovaSeq PE250 platform (according to the manufacturer's recommendations) provided by LC-Bio. Paired-end reads from the original DNA fragments were merged using FLASH. Alpha diversity and beta diversity were calculated by normalized to the same sequences randomly. The feature abundance was normalized using the relative abundance of each sample according to SILVA (release 132) classifier. Beta diversity was calculated using QIIME2, and the graphs were drawn using the R package (v3.5.2). Sequence alignment was performed using Blast, and the feature sequences were annotated with the SILVA database for each representative sequence.

Statistical analysis

All statistical analyses were performed using GraphPad Prism 8.0.2. Data are expressed as mean±SD (standard deviation) . A two-tailed Student's t-test, one-way or two-way ANOVA followed by Dunnett's post hoc test were used for testing differences among groups. A value of $P<0.05$ was considered statistically significant.

Supplementary Information

The online version contains supplementary material available at https://doi.org/10.1186/s12951-024-02749-1.

Supplementary Material 1

Acknowledgements
Not applicable.

Author contributions
L.C: investigation; methodology; formal analysis; validation; writing—original draft. D.D: investigation; methodology; formal analysis; validation. J.P: visualization; supervision; funding acquisition. R.L: investigation; methodology. Q.C: investigation; methodology. X.L: investigation; methodology. Y.G: investigation; methodology; supervision. J.L: investigation. K.L: investigation. Y.L: investigation. W.Z: methodology. S.L: methodology. X.Z: funding acquisition; project administration. Y.Z: conceptualization; visualization; writing—review and editing; supervision; funding acquisition; project administration. All authors read and approved the final manuscript.

Funding
This work was supported by National Natural Science Foundation of China (Grants 91959114, 81872106, 82272804), Scientific and Technological Research Program of Tianjin Municipal Education Commission (No. 2019ZD025), Natural Science Foundation of Tianjin (No. 22JCQNJC01700), Tianjin Science Fund for Distinguished Young Scholars (No. 20JCJQJC00270) and Scientific and Technological Research Program of Tianjin Health Commission (No. TJWJ2022XK015). This work was funded by Tianjin Key Medical Discipline (Specialty) Construction Project (No. TJYXZDXK-070 C), Tianjin Health Research Project (No. TJWJ2023QN018) and Youth Research Program of the Second Hospital of Tianjin Medical University (No. 2022ydey09, No. 2022ydey02).

Data availability
No datasets were generated or analysed during the current study.

Declarations

Ethics approval and consent to participate
All animal experiments were conducted following the Guidelines for Care and Use of Laboratory Animals of the Tianjin University of Traditional Chinese Medicine of China and were approved by the Animal Ethics Committee of the Tianjin University of Traditional Chinese Medicine (TCM-LAEC2023041).

Consent for publication
Not applicable.

Competing interests
The authors declare no competing interests.

Received: 22 February 2024 / Accepted: 2 August 2024
Published online: 13 August 2024

References

1. Collaborators GBDIBD. The global, regional, and national burden of inflammatory bowel disease in 195 countries and territories, 1990–2017: a systematic analysis for the global burden of Disease Study 2017. Lancet Gastroenterol Hepatol. 2020;5:17–30.
2. Kucharzik T, Ellul P, Greuter T, Rahier JF, Verstockt B, Abreu C, Albuquerque A, Allocca M, Esteve M, Farraye FA, et al. ECCO Guidelines on the Prevention, diagnosis, and management of infections in inflammatory bowel disease. J Crohns Colitis. 2021;15:879–913.
3. Lamb CA, Kennedy NA, Raine T, Hendy PA, Smith PJ, Limdi JK, Hayee B, Lomer MCE, Parkes GC, Selinger C, et al. British Society of Gastroenterology consensus guidelines on the management of inflammatory bowel disease in adults. Gut. 2019;68:s1–106.
4. Friedrich M, Pohin M, Jackson MA, Korsunsky I, Bullers SJ, Rue-Albrecht K, Christoforidou Z, Sathananthan D, Thomas T, Ravindran R, et al. IL-1-driven stromal-neutrophil interactions define a subset of patients with inflammatory bowel disease that does not respond to therapies. Nat Med. 2021;27:1970–81.
5. Cai Z, Wang S, Li J. Treatment of inflammatory bowel disease: a Comprehensive Review. Front Med (Lausanne). 2021;8:765474.
6. Xiao B, Xu Z, Viennois E, Zhang Y, Zhang Z, Zhang M, Han MK, Kang Y, Merlin D. Orally targeted delivery of Tripeptide KPV via Hyaluronic Acid-Functionalized nanoparticles efficiently alleviates Ulcerative Colitis. Mol Ther. 2017;25:1628–40.
7. Xiao B, Zhang Z, Viennois E, Kang Y, Zhang M, Han MK, Chen J, Merlin D. Combination therapy for Ulcerative Colitis: orally targeted nanoparticles prevent mucosal damage and relieve inflammation. Theranostics. 2016;6:2250–66.
8. Tontini GE, Vecchi M, Neurath MF, Neumann H. Advanced endoscopic imaging techniques in Crohn's disease. J Crohns Colitis. 2014;8:261–9.
9. Heine GD, Hadithi M, Groenen MJ, Kuipers EJ, Jacobs MA, Mulder CJ. Double-balloon enteroscopy: indications, diagnostic yield, and complications in a series of 275 patients with suspected small-bowel disease. Endoscopy. 2006;38:42–8.
10. Duigenan S, Gee MS. Imaging of pediatric patients with inflammatory bowel disease. AJR Am J Roentgenol. 2012;199:907–15.
11. Kilcoyne A, Kaplan JL, Gee MS. Inflammatory bowel disease imaging: current practice and future directions. World J Gastroenterol. 2016;22:917–32.
12. Wu Y, Briley K, Tao X. Nanoparticle-based imaging of inflammatory bowel disease. Wiley Interdiscip Rev Nanomed Nanobiotechnol. 2016;8:300–15.
13. Naha PC, Hsu JC, Kim J, Shah S, Bouche M, Si-Mohamed S, Rosario-Berrios DN, Douek P, Hajfathalian M, Yasini P, et al. Dextran-coated Cerium Oxide nanoparticles: a computed tomography contrast Agent for Imaging the gastrointestinal tract and inflammatory bowel disease. ACS Nano. 2020;14:10187–97.
14. Cao Y, Cheng K, Yang M, Deng Z, Ma Y, Yan X, Zhang Y, Jia Z, Wang J, Tu K, et al. Orally administration of cerium oxide nanozyme for computed tomography imaging and anti-inflammatory/anti-fibrotic therapy of inflammatory bowel disease. J Nanobiotechnol. 2023;21:21.
15. Min DK, Kim YE, Kim MK, Choi SW, Park N, Kim J. Orally Administrated inflamed Colon-targeted Nanotherapeutics for Inflammatory Bowel Disease treatment by oxidative stress level modulation in colitis. ACS Nano. 2023;17:24404–16.
16. Li H, Xia P, Pan S, Qi Z, Fu C, Yu Z, Kong W, Chang Y, Wang K, Wu D, Yang X. The advances of Ceria nanoparticles for Biomedical Applications in Orthopaedics. Int J Nanomed. 2020;15:7199–214.
17. Dos Santos AM, Carvalho SG, Meneguin AB, Sabio RM, Gremiao MPD, Chorilli M. Oral delivery of micro/nanoparticulate systems based on natural polysaccharides for intestinal diseases therapy: challenges, advances and future perspectives. J Control Release. 2021;334:353–66.
18. Liang D, Shen X, Han L, Ren H, Zang T, Tan L, Lu Z, Liao X, Vetha BSS, Liu Y, et al. Dual-ROS sensitive moieties Conjugate inhibits Curcumin oxidative degradation for Colitis Precise Therapy. Adv Healthc Mater. 2024;13:e2303016.
19. Rahiman N, Markina YV, Kesharwani P, Johnston TP, Sahebkar A. Curcumin-based nanotechnology approaches and therapeutics in restoration of autoimmune diseases. J Control Release. 2022;348:264–86.
20. Sardou HS, Vosough PR, Abbaspour M, Akhgari A, Sathyapalan T, Sahebkar A. A review on curcumin colon-targeted oral drug delivery systems for the treatment of inflammatory bowel disease. Inflammopharmacology. 2023;31:1095–105.
21. Burge K, Gunasekaran A, Eckert J, Chaaban H. Curcumin and Intestinal Inflammatory diseases: Molecular mechanisms of Protection. Int J Mol Sci 2019, 20.
22. Kotla NG, Burke O, Pandit A, Rochev Y. An orally administrated Hyaluronan Functionalized Polymeric hybrid nanoparticle system for Colon-specific drug delivery. Nanomaterials (Basel) 2019, 9.
23. Marinho A, Nunes C, Reis S. Hyaluronic acid: a key ingredient in the therapy of inflammation. Biomolecules 2021, 11.
24. Kimura M, Maeshima T, Kubota T, Kurihara H, Masuda Y, Nomura Y. Absorption of orally administered Hyaluronan. J Med Food. 2016;19:1172–9.
25. Jing W, Zhu M, Wang F, Zhao X, Dong S, Xu Y, Wang S, Yang J, Wang K, Liu W. Hyaluronic Acid-Melatonin nanoparticles improve the Dysregulated Intestinal Barrier, Microbiome and Immune Response in mice with Dextran Sodium Sulfate-Induced Colitis. J Biomed Nanotechnol. 2022;18:175–84.
26. Mao T, Su CW, Ji Q, Chen CY, Wang R, Vijaya Kumar D, Lan J, Jiao L, Shi HN. Hyaluronan-induced alterations of the gut microbiome protects mice against Citrobacter rodentium infection and intestinal inflammation. Gut Microbes. 2021;13:1972757.

27. Lee Y, Sugihara K, Gillilland MG 3rd, Jon S, Kamada N, Moon JJ. Hyaluronic acid-bilirubin nanomedicine for targeted modulation of dysregulated intestinal barrier, microbiome and immune responses in colitis. Nat Mater. 2020;19:118–26.
28. Xiao B, Zhang M, Viennois E, Zhang Y, Wei N, Baker MT, Jung Y, Merlin D. Inhibition of MDR1 gene expression and enhancing cellular uptake for effective colon cancer treatment using dual-surface-functionalized nanoparticles. Biomaterials. 2015;48:147–60.
29. Kapoor DN, Bhatia A, Kaur R, Sharma R, Kaur G, Dhawan S. PLGA: a unique polymer for drug delivery. Ther Deliv. 2015;6:41–58.
30. Doggui S, Sahni JK, Arseneault M, Dao L, Ramassamy C. Neuronal uptake and neuroprotective effect of curcumin-loaded PLGA nanoparticles on the human SK-N-SH cell line. J Alzheimers Dis. 2012;30:377–92.
31. Hou Y, Jin J, Duan H, Liu C, Chen L, Huang W, Gao Z, Jin M. Targeted therapeutic effects of oral inulin-modified double-layered nanoparticles containing chemotherapeutics on orthotopic colon cancer. Biomaterials. 2022;283:121440.
32. Lei C, Liu XR, Chen QB, Li Y, Zhou JL, Zhou LY, Zou T. Hyaluronic acid and albumin based nanoparticles for drug delivery. J Control Release. 2021;331:416–33.
33. Van De Walle J, Hendrickx A, Romier B, Larondelle Y, Schneider YJ. Inflammatory parameters in Caco-2 cells: effect of stimuli nature, concentration, combination and cell differentiation. Toxicol Vitro. 2010;24:1441–9.
34. Vafaei SY, Esmaeili M, Amini M, Atyabi F, Ostad SN, Dinarvand R. Self assembled hyaluronic acid nanoparticles as a potential carrier for targeting the inflamed intestinal mucosa. Carbohydr Polym. 2016;144:371–81.
35. Cormode DP, Naha PC, Fayad ZA. Nanoparticle contrast agents for computed tomography: a focus on micelles. Contrast Media Mol Imaging. 2014;9:37–52.
36. Guo J, Li D, Tao H, Li G, Liu R, Dou Y, Jin T, Li L, Huang J, Hu H, Zhang J. Cyclodextrin-derived intrinsically bioactive nanoparticles for treatment of Acute and Chronic Inflammatory diseases. Adv Mater. 2019;31:e1904607.
37. Li Q, Zhang C, Zhu M, Shan J, Qian H, Ma Y, Wang X. W-GA nanodots restore intestinal barrier functions by regulating flora disturbance and relieving excessive oxidative stress to alleviate colitis. Acta Biomater. 2024;182:260–74.
38. Zhang C, Li Q, Shan J, Xing J, Liu X, Ma Y, Qian H, Chen X, Wang X, Wu LM, Yu Y. Multifunctional two-dimensional Bi(2)Se(3) nanodiscs for anti-inflammatory therapy of inflammatory bowel diseases. Acta Biomater. 2023;160:252–64.
39. Zhang C, Li Q, Xing J, Yang Y, Zhu M, Lin L, Yu Y, Cai X, Wang X. Tannic acid and zinc ion coordination of nanase for the treatment of inflammatory bowel disease by promoting mucosal repair and removing reactive oxygen and nitrogen species. Acta Biomater. 2024;177:347–60.
40. Jin T, Lu H, Zhou Q, Chen D, Zeng Y, Shi J, Zhang Y, Wang X, Shen X, Cai X. H(2) S-Releasing versatile Montmorillonite Nanoformulation Trilogically renovates the Gut Microenvironment for Inflammatory Bowel Disease Modulation. Adv Sci (Weinh). 2024;11:e2308092.
41. Korsvik C, Patil S, Seal S, Self WT. Superoxide dismutase mimetic properties exhibited by vacancy engineered ceria nanoparticles. Chem Commun (Camb) 2007:1056–8.
42. Heckert EG, Karakoti AS, Seal S, Self WT. The role of cerium redox state in the SOD mimetic activity of nanoceria. Biomaterials. 2008;29:2705–9.
43. Pirmohamed T, Dowding JM, Singh S, Wasserman B, Heckert E, Karakoti AS, King JE, Seal S, Self WT. Nanoceria exhibit redox state-dependent catalase mimetic activity. Chem Commun (Camb). 2010;46:2736–8.
44. Das M, Patil S, Bhargava N, Kang JF, Riedel LM, Seal S, Hickman JJ. Autocatalytic ceria nanoparticles offer neuroprotection to adult rat spinal cord neurons. Biomaterials. 2007;28:1918–25.
45. Venkataranganna MV, Rafiq M, Gopumadhavan S, Peer G, Babu UV, Mitra SK. NCB-02 (standardized curcumin preparation) protects dinitrochlorobenzene-induced colitis through down-regulation of NFkappa-B and iNOS. World J Gastroenterol. 2007;13:1103–7.
46. Guo X, Xu Y, Geng R, Qiu J, He X. Curcumin alleviates Dextran Sulfate Sodium-Induced colitis in mice through regulating gut microbiota. Mol Nutr Food Res. 2022;66:e2100943.
47. Kostic AD, Xavier RJ, Gevers D. The microbiome in inflammatory bowel disease: current status and the future ahead. Gastroenterology. 2014;146:1489–99.
48. Madsen KL, Doyle JS, Jewell LD, Tavernini MM, Fedorak RN. Lactobacillus species prevents colitis in interleukin 10 gene-deficient mice. Gastroenterology. 1999;116:1107–14.
49. Galdeano CM, Perdigon G. The probiotic bacterium Lactobacillus casei induces activation of the gut mucosal immune system through innate immunity. Clin Vaccine Immunol. 2006;13:219–26.
50. Geier MS, Butler RN, Giffard PM, Howarth GS. Lactobacillus fermentum BR11, a potential new probiotic, alleviates symptoms of colitis induced by dextran sulfate sodium (DSS) in rats. Int J Food Microbiol. 2007;114:267–74.
51. Sartor RB. Therapeutic manipulation of the enteric microflora in inflammatory bowel diseases: antibiotics, probiotics, and prebiotics. Gastroenterology. 2004;126:1620–33.
52. Oliva S, Di Nardo G, Ferrari F, Mallardo S, Rossi P, Patrizi G, Cucchiara S, Stronati L. Randomised clinical trial: the effectiveness of Lactobacillus reuteri ATCC 55730 rectal enema in children with active distal ulcerative colitis. Aliment Pharmacol Ther. 2012;35:327–34.
53. Zhang Z, Wu X, Cao S, Cromie M, Shen Y, Feng Y, Yang H, Li L. Chlorogenic acid ameliorates experimental colitis by promoting growth of Akkermansia in mice. Nutrients 2017, 9.
54. Zeng L, Cheng H, Dai Y, Su Z, Wang C, Lei L, Lin D, Li X, Chen H, Fan K, Shi S. In vivo Regenerable Cerium Oxide Nanozyme-loaded pH/H2O2-Responsive nanovesicle for Tumor-targeted Photothermal and Photodynamic therapies. ACS Appl Mater Interfaces. 2021;13:233–44.
55. Wirtz S, Popp V, Kindermann M, Gerlach K, Weigmann B, Fichtner-Feigl S, Neurath MF. Chemically induced mouse models of acute and chronic intestinal inflammation. Nat Protoc. 2017;12:1295–309.
56. Cheng S, Shen H, Zhao S, Zhang Y, Xu H, Wang L, Di B, Xu L, Hu C. Orally administered mesoporous silica capped with the cucurbit[8]uril complex to combat colitis and improve intestinal homeostasis by targeting the gut microbiota. Nanoscale. 2020;12:15348–63.
57. Sun Q, Luan L, Arif M, Li J, Dong QJ, Gao Y, Chi Z, Liu CG. Redox-sensitive nanoparticles based on 4-aminothiophenol-carboxymethyl inulin conjugate for budesonide delivery in inflammatory bowel diseases. Carbohydr Polym. 2018;189:352–9.
58. Logue JB, Stedmon CA, Kellerman AM, Nielsen NJ, Andersson AF, Laudon H, Lindstrom ES, Kritzberg ES. Experimental insights into the importance of aquatic bacterial community composition to the degradation of dissolved organic matter. ISME J. 2016;10:533–45.

Publisher's Note